REPORT DOCUMENTATION PAGE

AFRL-SR-AR-TR-04-

0147

1. REPORT DATE (DD-MM-YYYY)	2. REPORT DATE	3. DATES COVERED (From - To)
01-12-2003	FINAL	06/01/2001 to 12/01/2003

4. TITLE AND SUBTITLE
BIOLOGICAL AND SILICON MODELING OF MOVING TARGET DETECTION IN INSECTS

5a. CONTRACT NUMBER
F49620-01-C-0030

5b. GRANT NUMBER

5c. PROGRAM ELEMENT NUMBER

6. AUTHOR(S)
PATRICK SHOEMAKER
DAVID O'CARROLL

5d. PROJECT NUMBER

7. PERFORMING ORGANIZATION NAME(S) AND ADDRESS(ES)
TANNER RESEARCH, INC.
2650 EAST FOOTHILL BLVD.
PASADENA, CA 91107

8. PERFORMING ORGANIZATION REPORT NUMBER
Contract F49620-01-C-0030 Final Report

9. SPONSORING/MONITORING AGENCY NAME(S) AND ADDRESS(ES)
USAF, AFRL
AF OFFICE OF SCIENTIFIC RESEARCH
4015 WILSON BLVD., ROOM 713
ARLINGTON, VA 22203-1954
DR. WILLIAM LARKIN (703) 696-7297

10. SPONSOR/MONITOR'S ACRONYM(S)
USAF, AFRL, AFOSR

11. SPONSORING/MONITORING AGENCY REPORT NUMBER

12. DISTRIBUTION AVAILABILITY STATEMENT
DISTRIBUTION STATEMENT A. APPROVED FOR PUBLIC RELEASE; DISTRIBUTION IS UNLIMITED.

13. SUPPLEMENTARY NOTES

14. ABSTRACT

In this project, we studied the physiology of a class of visual neurons that we have labeled small target, movement detectors (STMDs), which respond selectively to small moving visual targets. In-vivo intracellular recordings were made in several model species (the hoverfly Eristalis tenax and the dragonflies Hemicordulia tau and Aeshna multicolor), while subject to moving visual displays. We found some STMD neurons are capable of responding selectively to small moving targets against moving cluttered backgrounds. We characterized the receptive field properties of a class of small-field STMDs that we labeled 'elementary small target movement detectors' (ESTMDs), which may be an early stage in a hierarchy of STMD processing. Models were developed for aspects of the processing performed by STMD neurons, and tested in simulations. In particular, a model for the ESTMD was developed and implemented in analog VLSI silicon.

15. SUBJECT TERMS
Insect vision, visual motion detection, moving target detection, intracellular recording, receptive field

16. SECURITY CLASSIFICATION OF:			17. LIMITATION OF ABSTRACT	18. NUMBER OF PAGES	19a. NAME OF RESPONSIBLE PERSON
a. REPORT	b. ABSTRACT	c. THIS PAGE			KEVIN DINNIENE
U	U	U	SAR	54	19b. TELEPONE NUMBER (*Include area code*) 626 432-5778

Contract F49620-01-C-0030

Biological and Silicon Modeling of Moving Target Detection in Insects

Final Report
1 December 2003

Patrick Shoemaker
David O'Carroll

Tanner Research, Inc.
2650 East Foothill Blvd.
Pasadena, CA 91107

Biological and Silicon Modeling of Moving Target Detection in Insects

Executive Summary

In this project, we studied the physiology of a class of visual neurons that we have labeled small target, movement detectors (STMDs), found in the third optic ganglion of insect species of several orders, which are notable for the aerial pursuit of prey or conspecifics. These neurons have selective responses for small moving targets in various parts of the animals' visual fields. In addition, we developed models for aspects of the processing performed by these cells, and designed and fabricated analog integrated circuits based on these models.

In the neurobiological portion of our work, the primary experimental tool we used was *in-vivo* intracellular recording in animals of the model species (the hoverfly *Eristalis tenax* and the dragonflies *Hemicordulia tau* and *Aeshna multicolor*), while subject to moving visual displays. We characterized the responses of a range of neurons that can be considered small target movement detectors; developed preliminary classifications for some of these cells, including a small-field STMD that we have labeled an 'elementary small target movement detector', or ESTMD, and which may be an early or intermediate stage in a hierarchy of STMD processing; discovered that at least some STMD neurons are capable of responding selectively to small moving targets against moving cluttered backgrounds; and obtained data from an STMD neuron that we believe will prove identifiable from individual to individual of a particular species (*E. tenax*).

In our modeling work, we developed both conceptual and numerical models for aspects of STMD processing. Simulations were performed using the tools MatLab and SPICE, in which time-domain stimuli (in many cases the same or similar to that presented to insects during experiments) were used as inputs. We modeled the processing performed by ESTMDs; studied the responses of elementary motion detectors (the putative front-end processors for subsequent for STMD neurons) to small target motion; developed a model for processing that could endow STMD neurons with selectivity for small target size in the direction of motion; examined possible mechanisms for collation of ESTMD outputs; and developed a revised hierarchy of STMD processing in view of the discovery of neurons capable of distinguishing moving targets against moving backgrounds.

In our effort to implement neuromorphic analog circuit models of STMDs, we evaluated primitive devices and STMD models in two different CMOS processes (standard bulk silicon mixed-signal CMOS and silicon-on-sapphire); invented a novel log-domain filter circuit that can be operated in a nonlinear mode to mimic the 'tonic' or persistent response property of ESTMD neurons; implemented, tested and demonstrated silicon models for the ESTMD; and implemented and performed pilot testing of a model for dendritic collation in a wide-field STMD analog.

1 INTRODUCTION

1.1 Background

1.2 Objectives

The stated objectives of the proposed work were:

1. Development of a biological model of insect small target, movement detector neurons (STMDs) to a sufficiently quantitative and abstract state to allow an artificial system to be based upon its principles of operation;
2. Demonstration of the feasibility of an artificial STMD implementation, in the form of an analog silicon model.

Although the work came to focus on particular classes of STMD cells and aspects of their behavior, the two stated objectives of the original proposal remained fundamentally unchanged. However, as the work progressed, the range of STMD neurons found made evident the need for further basic characterization of these cells and their physiologcal characteristics, and this became an additional *de facto* objective of the experimental part of the effort.

1.3 Approach

Our work has involved experimental neurobiology, numerical modeling and simulation, and development of analog silicon models of STMD functions. The primary experimental tool has been *in-vivo* intracellular recording from putative STMD neurons in intact animals (dragonflies and hoverflies) while subject to stimulation via a visual display. In parallel with experimental neurophysiology, modeling and simulation was conducted at several levels: both biologically detailed and higher-level, abstract models were developed. This paradigm generates testable hypotheses for experimental verification, and promotes the abstraction of essential computational principles that underlie physiological responses. Silicon models have built upon the results of simulation-based modeling. STMD models were fabricated in analog integrated circuitry using submicron, mixed-signal CMOS processes, and neuromorphic design techniques.

2 METHODS AND PROCEDURES

2.1 Experimental Neurobiology

The major experimental tool for this project has been *in-vivo* intracellular recording in intact animals while they are subject to stimulation via a visual display. The species used in the preparations have been the dragonflies *Aeshna multicolor* and *Hemicordulia tau* (order Odonata), and the hoverfly *Eristalis tenax* (order Diptera), all animals that locate and pursue prey or conspecifics visually. During the experimental procedure, the animals are immobilized, a small portion of the rear head capsule is removed, and a

drawn quartz or aluminosilicate glass microelectrode filled with electrolyte solution, with a tip of less than 100nm diameter, is inserted to penetrate individual neurons. A reference electrode (fine gauge silver chloride coated silver wire), is inserted into the rear of the eye contralateral to that from which recordings are obtained. The potential difference between this reference and the internal membrane potential of the recorded cell is digitized as moving visual scenarios are displayed to the animal on a CRT screen.

Data recorded during such experiments were analyzed, and electrophysiological events such as changes in graded potential or rate of firing of action potentials were correlated with events (in particular, small target motion) in the stimulus sequence. As the project progressed and hypotheses regarding the processing performed by STMD neurons were generated, specialized stimulus sequences were developed for further experiments.

Considerable effort was expended during the course of the project on two major technical issues relating to the experimental preparation and procedures: one had to do with improving the stability and quality of the electrophysiological data, and the second with advancing stimulus display capabilities.

Successful recording from STMD neurons is more difficult than from the large, wide-field tangential cells in the lobula plate which have been a staple of insect vision research in ours as well as other laboratories. Our work with STMD cells has spurred the development of specialized techniques during the course of the project. Initial recording attempts were hampered by signal degradation due to electrical noise intruding into recordings. Much of this noise emanates from the computer display on which stimuli are presented, which, given its proximity to the recording site, presents a substantial challenge to shielding. In recordings from tangential cells, noise has not been a major issue, since we are able to low-pass filter the electrical response from these cells (which are non-spiking), and to use relatively low-impedance recording electrodes (ca. 50-70 MΩ). STMD neurons are generally much smaller than tangential cells. Preliminary analysis of recorded cells after dye injection suggests that our recordings *in vivo* are often from neural processes below 200nm diameter, necessitating the use of extremely fine microelectrodes. Our initial recording attempts from STMDs with the low impedance electrodes were partially successful, in that we were able to penetrate neurons that responded to small targets, but we 'lost' cells after a short recording period (<1 minute), possibly due to damage caused by the electrode tip as it first penetrates the cell. We subsequently developed modified programs on our Sutter P-97 electrode puller to fabricate finer-tipped electrodes, which give more stable recordings from STMD cells (although the recording duration is still typically minutes in duration rather than the hours that can be achieved with tangential cells). Unfortunately, the higher impedance (120-180MΩ) of these electrodes is poorly matched to the preamplifier head stage and results in additional noise pickup.

This problem is exacerbated by the fact that most STMD neurons fire 'fast' action potentials (<1 ms duration for the positive phase), which require a much higher sample rate (5 kHz) to digitize reliably and which therefore preclude the same degree of low-pass filtering that is acceptable for tangential cell recordings. Since the noise from the display is at relatively high frequencies, this leads to worsening of the recording signal-to-noise ratio. We have tackled this problem by careful attention to electrical shielding, including the use of a grounded transparent thin-film metallic acetate material (Tecknit) material

that reduces noise emanation through the CRT. One tradeoff with this approach is that this screen reduces the mean luminance of the display by a factor of two. This is of concern since the display luminance is already much lower than that of the typical sky against which targets would be viewed in nature. While a brighter display would have been desirable, we were not successful in locating a suitable high-speed bright-phosphor CRT display during the course of the project. Any CRT used in these experiments must be capable of a 200 frame per second vertical refresh (frame rate) in order to exceed the flicker fusion frequency in the temporally acute insect eye.

During the first half of the project, we were also best by an intermittent low-frequency noise problem, eventually traced to a break-down of the Ag-AgCl coating placed on our reference (ground) electrodes. This layer is formed on silver wire by electroplating. Upon further reading on this subject we found that AgCl layer instability could have resulted from the relatively high voltage (9V) we were using to coat the silver wire: we found that reducing the potential during coating to 1.5 Volts produces a more stable AgCl layer and this led to a complete elimination of the intermittent low-frequency noise.

Generation of display stimuli for the experiments was also a significant technical challenge. All of our preliminary neurobiological data were obtained using relatively dated stimulus display techniques, including a Picasso image synthesizer and a Cambridge Research Systems VSG display card. These proprietary systems are expensive and have many limitations for particular applications, but are necessary to produce the very high frame rates required for simulation of moving scenes and patterns when working with insects. However, during the course of the project, Andrew Straw, a graduate student in the O'Carroll laboratory, developed a new display system, the "Vision Egg," under partial support of this contract.

Computer graphics capabilities have been driven in recent years by the requirements of commercial computer games, and the latest generation AGP-based graphics cards that are now standard in modern computers have capabilities that exceed those of the traditional display systems used by vision scientists. They are capable of drawing very complex scenes at high frame rates. The Vision Egg is a programming library that uses these standard, inexpensive computer graphics cards to produce visual stimuli for vision research experiments. It allows programming of the cards with OpenGL, an open-source standard for computer graphics programming. Potentially difficult tasks, such as initializing graphics, getting precise timing information, controlling stimulus parameters in real-time, and synchronizing with data acquisition, are expedited by routines within the Vision Egg library. The Vision Egg is an open-source project licensed under the GNU GPL. To facilitate distribution to the vision science community, we have published it on an open source web site, http://www.visionegg.org. Evaluation copies of the code can be freely downloaded by other vision scientists.

Using the Vision Egg, we have developed a progressively more sophisticated repertoire of stimulus capabilities during the course of the project, progressing from a small target drifting unidirectionally against a blank screen, to a small target moving along arbitrary paths (such as orbits) against cluttered backgrounds (including natural imagery), to small targets moving against drifting cluttered backgrounds with interactive selection of target location in the scene.

Finally, we have improved data acquisition techniques and hardware, by writing data acquisition code in Matlab, procuring a new (National Instruments) data acquisition card that offers substantial noise advantages over the prior GWI-625 card used in our laboratory, and integrating these with the Vision Egg for purposes of sychronization of display with data acquisition.

2.2 Modeling and Simulation

Conceptual models for the processing performed by particular STMD neurons were developed and refined as experimental work proceeded during the project. As these models became sufficiently well-defined that they could be expressed mathematically, they were coded in software, and simulations were performed to verify their response characteristics and investigate their behaviors. This process eventually generated testable hypotheses which in some instances could be used as feedback for the neurobiology task, to design experiments for more detailed investigation of STMD physiology.

Numerical modeling and simulation were performed in several environments. In general, the various simulation tools were used to compute transient time-domain responses of dynamic systems corresponding to the STMD models, to particular simulated stimuli (in some cases, the same stimuli that were presented to subject animals during experiments). The academic investigator conducted simulations in which the models maintained a relatively high degree of fidelity to the biological system, primarily using the mathematical package Matlab with custom-written code. Modeling of a more abstract nature was carried out by the commercial partner using the tool SPICE (Simulation Program with Integrated Circuit Emphasis). SPICE is based on circuit representations, but admits the use of purely abstract components in addition to models of particular electronic devices. In SPICE simulations, we attempted to verify what we believed to be the essential computational features of STMD processing seen and modeled in the biological neurons. Finally, SPICE also served as a platform for device-based circuit models during the process of circuit design. Simulations of the circuits actually implemented in the silicon modeling task were performed (or at least attempted) in order to verify their response characteristics.

It is presumed that considerable early visual and motion processing takes place in the visual pathway prior to the STMD neurons, and some simulations (with biological models in particular) attempted to account for this processing by including it in the modeling in order to form realistic input signals for the STMDs themselves. We have assumed as a starting hypothesis that elementary motion detectors (EMDs) form the principal inputs for STMD processing, and in fact, a substantial effort was devoted to simulating the responses of the EMDs themselves to the passage of small moving objects, in order to understand the characteristics of their responses that might be particular to the scenario of interest.

The processing leading up to the EMD output, as implemented in our simulations, can be summarized as follows. The compound eye optics, in accordance with prior studies, were assumed to have a blurring or spatial lowpass characteristic with a spatial constant or half-width on the order of the inter-ommatidial separation. Photoreceptors were assumed to perform a roughly logarithmic transformation on the received light intensity, and to have a predominantly lowpass temporal characteristic. This logarithmic

dependence was in some cases replaced with a more detailed model such as the Naka-Rushton or Lipetz model [4][6]. In the lamina, further temporal filtering with a predominantly bandpass characteristic was assumed to occur. Next, the EMD was represented with the correlational or Reichardt model [1][2]. Frequently, this model was elaborated with biologically realistic features, such as saturating nonlinearities in the signal path. Finally, in accordance with the work of O'Carroll et al. [1][7], contrast gain control was in some instances implemented in conjunction with the EMD.

In other simulations, additional preprocessing of some kind not explicitly simulated was assumed to take place, and the inputs to a particular stage of STMD processing were assigned certain characteristics. For instance, we assumed in some simulations that signals from EMDs had been prefiltered for events consistent with the passage of a small moving target, and that this prefiltering resulted in an excitatory burst or pulse of a constant amplitude when such an event occurred.

Preliminary processing from early vision through the EMD, and the first stages of small target detection as well, were modeled as taking place on retinotopic arrays of processors. Initially, simulations were performed with small, rectangular arrays, and with uniaxial motion. However, before the end of the project, we developed tools to resample moving imagery from standard video formats onto hexagonal arrays analogous to the actual geometry of photoreceptors in the compound eye, and to perform simulations with two-dimensional motion using such arrays. (Work by O'Carroll and Shoemaker in this area received substantial support from a concurrent SBIR project (Navy contract N00014-03-M-0171), while work by DuBois in the O'Carroll lab was supported by this contract.)

2.3 Circuit Design, Implementation, and Testing

Based on models developed for the processing performed by STMD cells, we developed experimental analog circuits to implement functions observed in biological STMD neurons. In the spirit of Mead and coworkers [5], we focused on micropower or subthreshold MOS devices, relying primarily on the computational primitives available in that regime. In addition to physical modeling of functions associated with moving target detection, we considered limitations of microelectronic technology (in particular, matching of device characteristics from transistor to transistor) that have the potential to negatively impact robust, large-scale practical implementations in the future.

For flexibility, we chose in the early portion of the project to evaluate multiple submicron CMOS processes as potential media for implementation of our models. The processes considered were accessed via the MOSIS prototyping service. Initially, we selected a standard mixed-signal bulk CMOS process (TSMC 0.35μm), and a silicon-on-sapphire (SOS) process (Peregrine Semiconductor 0.5μm) in which devices are fabricated in a thin silicon film on insulating substrate. The SOS process results in dielectric isolation of transistors, and allows fabrication of a number of primitive devices unavailable in bulk silicon. Prior to submission of circuits for fabrication, however, we elected to change vendors for bulk process and use the Agilent (formerly HP) 0.5μm mixed-signal CMOS process. This change was due to receipt of information suggesting superiority of device matching characteristics in the Agilent process.

Our approach consisted of the design, submission, and test and evaluation of a series of test chips. These were intended to allow incremental development of devices and circuit concepts for STMD models. The chip design process comprises conceptual design, schematic entry, circuit simulation for more complex circuits, physical design (layout of mask data), verification (design rule checking of the layout and comparison with the schematics), and transport of the layout data to the vendor (MOSIS). Simulations of higher level functions associated with implemented STMD models are discussed in the sections in Modeling and Simulation (2.2 and 3.2).

2.3.1 Early Test Devices

Early in the project, an unplanned opportunity arose to place some devices and circuits on an SOS chip fabricated under other funding, and to evaluate some existing devices on yet another SOS chip. We focused on evaluating primitive devices that were considered to be of potential use in future silicon models of STMDs. As mentioned above, a number of such devices are not feasible in an ordinary bulk process, and because these were typically non-standard even in SOS, we developed technology files for our design environment allowing representation and extraction of all novel devices. These files include a library of schematic symbols for entry of schematic circuit diagrams, and a layout file with layer definitions allowing the physical design of the novel devices and extraction for verification.

Ultimately, the primitive devices placed on the gratis SOS test chip included:

- MOSFETs with body connections that are also operable as gated lateral bipolar junction transistors (BJTs), in both edged and edgeless configurations;
- Ungated lateral BJTs;
- Depletion-mode MOSFETs (useful for self-biasing above-threshold circuits and moderately high resistors);
- Depletion capacitors for implementation of relatively linear, high-value capacitances.

Some simple multi-transistor circuits were also placed on the chip, including lossless BJT current mirrors with MOSFET base drivers, and a simple log-domain low-pass current filter that was expected to allow implementation of very long time constants. The gratis chip was submitted in early October 2001.

2.3.2 Chip 1

Subsequently, we designed a pair of test chips for submission to both the bulk CMOS and SOS processes. (These first two chips contained some circuits in common with a closely-related, Air-Force-funded project (SBIR contract F08630-02-C-0013), and fabrication costs were shared between the two projects.)

The silicon-on-sapphire test chip, ***chip_1_sos***, was submitted to a MOSIS / Peregrine Semiconductor fabrication run closing 6 May 2002. The primary circuit on this chip was an array of 'elementary small target motion detectors,' or ESTMDs, a concept based on experimental results and analysis from a class of small-field STMD neurons studied experimentally during the project (see Sections 3.1.3 and 3.2 below). Addressing circuitry for purposes of handling inputs to this array was also integrated with the circuit.

The chip also contained a number of subcircuits and devices of interest, including test structures to evaluate:

- MOS transistor matching (devices with regular and light channel dopings)
- MOS transistor leakage currents, in edged and edgeless devices (this limits the time constants attainable in dynamic circuits)
- Lateral bipolar junction transistor (BJT) characteristics and performance (npn & pnp devices; gated and ungated; all possible base dopings)
- Lateral BJT matching (light base dopings, regarded as the most potentially useful)
- Log-domain lowpass and highpass filters (for very long time constants)
- A Gm-C lowpass filter
- Miscellaneous small building-block circuits (e.g., differential pairs, current mirrors)

The physical layout of this chip is depicted below in Figure 1:

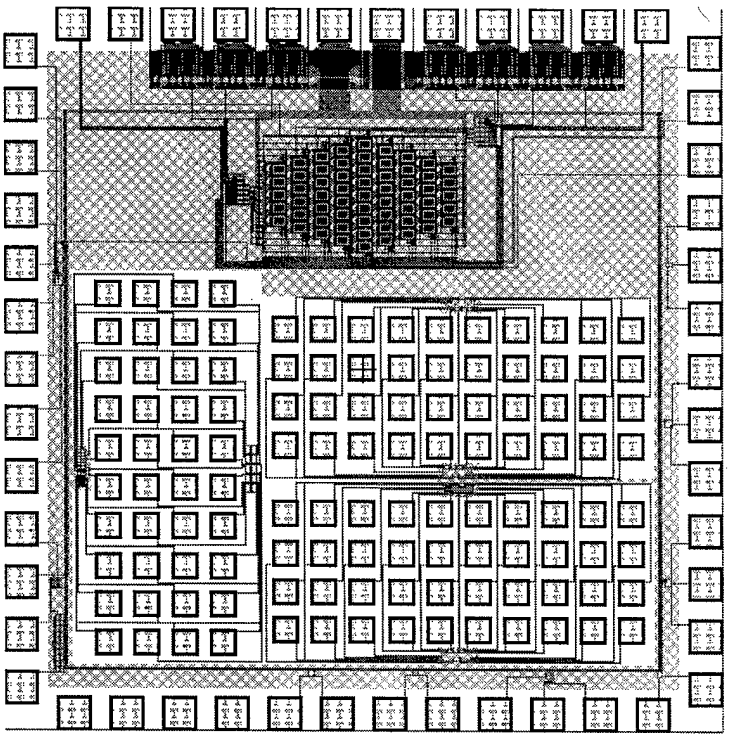

Figure 1: Physical layout of *chip_1_sos.*

In Figure 1, the hexagonal array at top is the ESTMD array, while the lower central portion contains individual test devices. Multi-transistor test circuits were arrayed around the perimeter, connecting to the outer ring of bonding pads. Because the number of bonding pads is limited, we addressed the I/O issue using a probe pad structure, in conjunction with a probe card allowing simultaneous contact to twenty probe pads for dc testing purposes. There are six such 20-pad structures for probing of individual test devices in the lower center of the chip. With these structures, unpackaged die could be placed on a probe station for testing.

The first bulk silicon test chip, ***chip_1_bulk***, was submitted to the MOSIS / Agilent fabrication run closing 1 July 2002. This chip contained an ESTMD array similar to that fabricated on the SOS chip, but modified for implementation in bulk silicon. It also included test structures to evaluate:

- MOS transistor matching (both standard pairs and common-centroid quads)
- Devices to investigate linear dimension effects on MOS transistor matching (i.e., length and width effects rather than area)
- Log-domain lowpass and highpass filters
- A long-time-constant lowpass filter based on linear current division technique with MOS transistors
- A Gm-C lowpass filter
- Miscellaneous small building-block circuits (e.g., differential pairs, current mirrors)

The physical layout of the chip is depicted below in Figure 2:

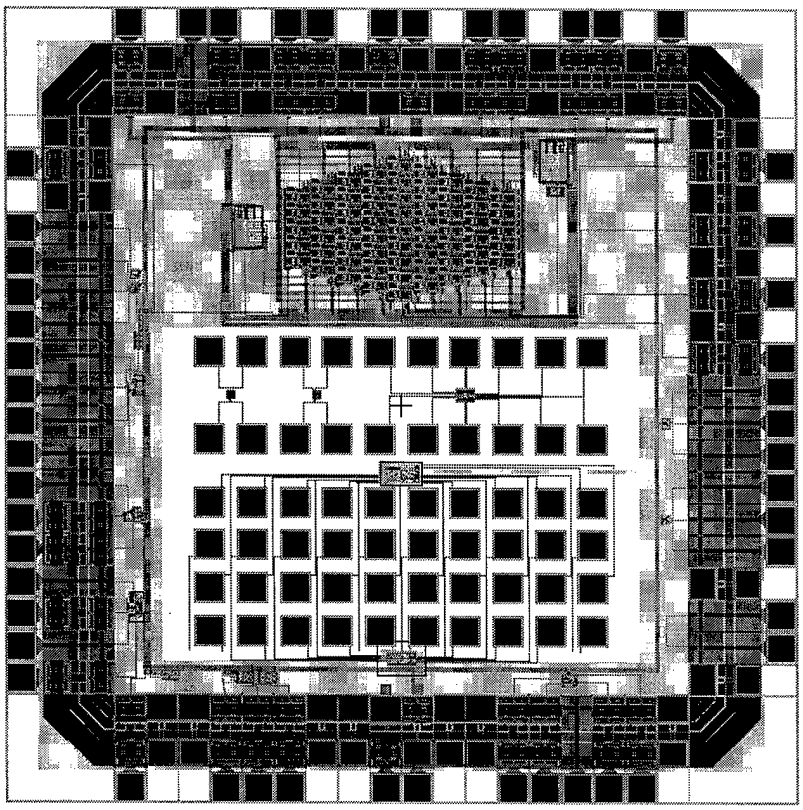

Figure 2: Physical layout of *chip_1_bulk*.

In Figure 2, the hexagonal array at top is the ESTMD array, while the lower central portion contains individual test devices. As on ***chip_1_sos***, multi-transistor test circuits were arrayed around the perimeter, and probe pad structures were used for individual devices. There are three 20-pad structures on ***chip_1_bulk***.

2.3.3 STMD Chip

Our research plan called for fabrication of a second, more advanced test chip following the initial pair. Based on test results, we decided that this chip would be fabricated in bulk CMOS only. Unfortunately, access to the Agilent process used for the first chip was discontinued by MOSIS in the interim, and we were forced to revert to the original TSMC 0.35μm bulk CMOS process. Because we had used MOSIS scalable design rules, translation of existing designs to the new process was not prohibitively difficult. The final chip, ***stmd_chip***, was completed and submitted on 23 June 2003. It contained two versions of ESTMD arrays with design revisions relative to the first submssion, and an analog of a wide-field STMD cell that collates inputs from an array of ESTMDs. It also included a set of transistor matching test structures and a revision of the log-domain lowpass filter appearing on the prior submission.

The physical layout of the chip is depicted below in Figure 3:

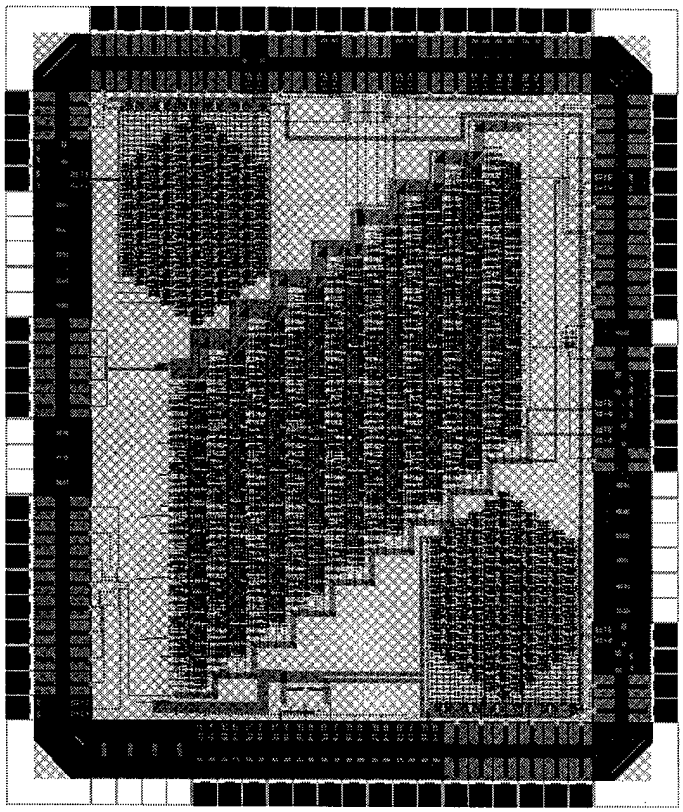

Figure 3: Physical layout of *stmd_chip*.

In Figure 3, the hexagonal arrays at top left and bottom right are the ESTMD arrays, while the central portion contains the integrated ESTMD arrays and wide-field neuron

analog. Further test structures are placed around the margins of the chip area that lies inside the bonding pad ring.

2.3.4 Testing

Following receipt of each chip from the foundry, test and evaluation was performed. A test board was assembled for each chip, including a socket for the device under test, as well as biasing and other auxiliary circuitry needed to operate it. In addition, a commercial field-programmable-gate-array (FPGA) integrated circuit and board were procured, and the FPGA was programmed to generate control signals necessary to dynamically address elements in the test arrays, in order to supply inputs that simulated 'moving objects', and also to generate control signals for purposes of data acquisition.

Finally, a 20-pin probe card and mounting hardware were procured, to allow contact to and testing of devices arrayed in probe structures on the first pair of chips. The probe card was mounted on the platen of a probe station resident in the Tanner Research hardware laboratory. Testing was carried out with standard laboratory bench instruments and computer-controlled data acquisition hardware at Tanner Research.

3 ACCOMPLISHMENTS AND NEW FINDINGS

3.1 Experimental Neurobiology

We consider our most significant accomplishments in neurobiology under support of this project to be: characterization of the responses of a range of neurons that can be considered STMDs; development of preliminary classifications for some of these cells, including a small-field STMD that we have labeled an 'elementary small target movement detector', or ESTMD, and which may be an early or intermediate stage in a hierarchy of STMD processing; the discovery of STMD neurons capable of responding selectively to small moving targets against moving cluttered backgrounds; and the finding of a neuron that we believe will prove identifiable from individual to individual of a particular species (*E. tenax*), according to both physiological and anatomical criteria.

3.1.1 General Properties of STMD Neurons

In our initial experiments, the visual stimuli applied to evaluate putative ESTMD neurons consisted of small targets moving against homogeneous static backgrounds, and additionally in control experiments, larger moving objects and moving gratings. In these experiments, we found that STMD neurons tend to be 'spiking' or action-potential-generating cells, and that a variety of neurons, with a range of receptive field properties, could be found in all of the subject species. (In addition to the species studied experimentally, O'Carroll and Henry also reviewed prior data obtained from putative STMD cells in a mantid, a predatory species from a third insect order, and found similar characteristics in those cells as well.) Some STMD neurons have small excitatory receptive fields (subtending a few degrees to perhaps ten degrees of visual angle), and some much larger receptive fields, from a few tens of degrees to the entire hemi-field viewed by an eye. The cells with largest receptive fields tend to have the most 'highly

tuned' response properties, characterized by no spontaneous firing activity, and no response to 'non-preferred' targets such as bars, edges or grating patterns. These cells do, however, respond very strongly to small targets (down to 0.5 x 0.5 degrees) that move at any location within the receptive field. The cells with smaller receptive fields typically display distinct response maxima at the center of those fields. These neurons tend to be slightly less selective for small target motion, giving weak (transient) responses to a variety of other stimuli. Interestingly, when the graded memebrane potentials of these neurons are observed, they show evidence of a complex receptive field structure, with a much larger, asymmetric inhibitory 'surround' region in addition to the excitatory 'center'. We also found some evidence, in the form of recordings from cells with similar response properties but spatially offset receptive fields, that individual neurons (particularly the smaller-field cells) may be retinotopically organized.

The general properties of STMD neurons deduced from these experiments include:

1. Long response latency (typically ca. 40-50 ms).
2. Strong selectivity for small targets.
3. Both direction selective and non-directional responses to target motion.
4. Variety of receptive field sizes.
5. Differences in velocity tuning: some sharply tuned for maximal response to a particular velocity, some monotonic.
6. Tendency for target direction selectivity in velocity tuned cells.
7. Direct relation between velocity optimum and target extent in the direction of motion, in velocity tuned cells.
8. Cells with largest receptive fields tend to have strongest selectivity for size, direction, and tend to lack any spontaneous activity.
9. Post-synaptic noise evident in some cells: IPSPs occur as lateral target extent is increased, with noisy 'breakthrough' EPSPs, suggesting 'competitive' recruitment of both excitatory and inhibitory pathways.
10. Post-synaptic noise is suppressed by wide-field motion (possibly pre-synaptic gating), suggesting more than one source of inhibitory feedback.

3.1.2 Wide-Field STMDS

STMD neurons were found to fall into two clear groups in terms of their tuning to target velocity: those with a distinct optimum speed ('velocity tuned') and those which give monotonically increasing responses up to the highest speeds tested (ca. 1000 degrees per second). Neither class of velocity tuning is an obvious emergent property from the array of elementary motion detectors that are assumed to form inputs to the STMDs, and they likely result from a combination of the inherent velocity tuning of EMDs and the dynamic properties associated with the receptive fields of STMDs themselves. This is further suggested by results of a similar experiment where we examined velocity tuning of an HS neuron (a wide-field motion detector) in response to small moving targets. Although they respond more weakly to this stimulus than to wide-field motion, non-linear spatial summation within their receptive fields (sometimes called 'gain control') means that they produce measurable responses to moderate sized targets (3 by 3 degrees). Surprisingly, the HS neuron shows no distinct velocity optimum, instead responding monotonically to increasing target speed to the highest velocities tested (ca. 300 degrees per second). By comparison, direction selective STMDs often (if not always) show a very

sharp peak in velocity tuning at much lower speeds. Furthermore, while STMD neurons show tuning that shifts to higher speeds as the longitudinal dimension of the target increases, the HS neuron does not.

The velocity-tuned wide-field STMD neurons can be further classified on the basis of their direction selectivity and velocity tuning into several sub-classes:

(1) Strongly direction-selective neurons with a low optimum target speed (ca. 30 degrees per second). [This class has been clearly identified in *Hemicordulia*, and we have preliminary evidence for these neurons in *Aeshna*].

(2) Strongly direction-selective neurons with a high optimum target speed (ca. 100 degrees per second or more). [This class has been clearly identified in *Aeshna*, and we have preliminary evidence for these neurons in *Hemicordulia*].

(3) Weakly direction-selective (or non-selective) neurons with a high optimum target speed (ca. 100 degrees per second or more). These cells tend to be slightly less selective for small target size than strongly direction-selective neurons. [This class has been clearly identified in both species].

We found no evidence for non-directional neurons with low velocity optima.

Experimental evidence with respect to these characteristics is not as complete for *Eristalis* as for the dragonfly species, but results so far are consistent with the same conclusions.

Some examples of response characteristics from a wide-field, velocity-tuned STMD are depicted below in Figure 4. These results depict, on the left, a direct relationship between longitudinal target size (i.e., extent in the direction of motion) and the optimum response velocity, and on the right, the selectivity of the cell for smallness of the target in the lateral direction (i.e., extent perpendicular to the direction of motion).

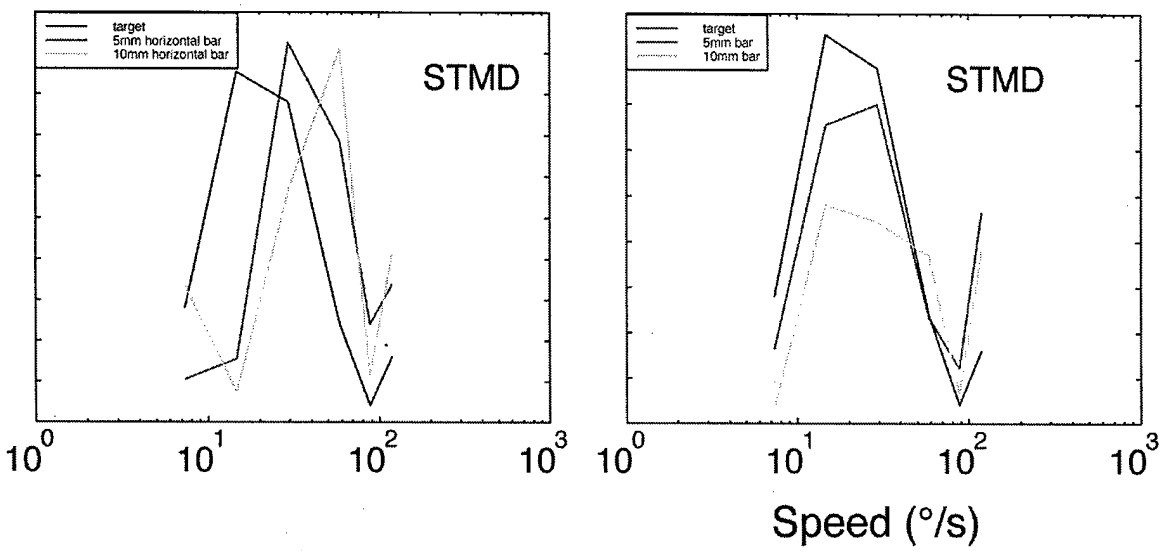

Figure 4: Velocity tuning at different stimulus sizes and target speeds. At left, response of an STMD in the dragonfly *Hemicordulia tau* to a small moving target as a function of target velocity, with the extent of the target in the direction of motion (the 'horizontal' direction) as a parameter. As the target becomes longer, the velocity tuning curves shift to higher optima At right, similar velocity tuning curves for an STMD in *H. tau* , but with lateral size of the target (i.e., extent perpendicular to the direction of motion) as a parameter. Lateral extent has no effect on tuning optima of the cell, only its general response level.

The clear evidence for at least two velocity optima among the direction-selective STMDs is an exciting finding. We propose that such a finding would be consistent with a possible role for the neurons in 'velocity parallax' - encoding target distance on the basis of apparent speed of targets during translatory motion by the dragonfly. Both *Aeshna* and *Hemicordulia* are so-called 'hawking' dragonflies, which initially detect target motion during hovering flight and then pursue prey aerially. Following detection of prey during hovering, these insects make a characteristic translation at moderate speed, before attempting target interception. During such translations, the two direction-selective STMD classes described above would respond differentially to the same target, even if that target were stationary, in a manner that depends only on target distance. A 'higher order' neuron could potentially integrate information from two or more of such neurons to produce a response that is velocity opponent (and thus distance opponent during self-motion).

3.1.3 The Putative Elementary Small Target Movement Detector

Further work and characterization of small-field STMDs led us to the conclusion that they might constitute a basic unit for small-target motion processing, an 'elementary small target motion detector' or ESTMD, perhaps serially hierarchical (i.e., pre-synaptic) to wide-field 'collator' cells corresponding to the wide-field STMD neurons. The receptive fields of putative ESTMD cells display very small excitatory centers, with larger and more diffuse inhibitory surrounds. The excitatory centers suggest that these

cells may receive excitatory inputs from only a few adjacent ommatidia (presumably via EMDs receiving input from those ommatidia). They typically have a much larger, asymmetric (offset or notched) inhibitory surround region, visible only in the graded potential of the cell as it is subject to small moving target stimuli. These cells tend to be direction selective, with a preferred direction always corresponding to the orientation of the offset surround: only a target that enters the receptive field through the 'notch' or weakest part of the inhibitory region is capable of eliciting sufficient excitation to cause the firing of a burst of action potentials.

An example of the receptive field of a putative ESTMD is shown below in Figure 5, recorded intracellularly from the lobula of a hoverfly *Eristalis*. In this plot, each rectangular sub-field represents the boundaries of the screen on which stimuli (small drifting targets) were displayed. The response of the neuron to targets moving from left to right (left panels) and then right to left (right panels) at a series of vertical positions on the screen (presented in random order) is plotted, with the vertical axis representing space and the horizontal axis time. The time axis is scaled equivalently to the spatial dimension, so that flipping the right panels about their vertical axes transforms the data back into space.

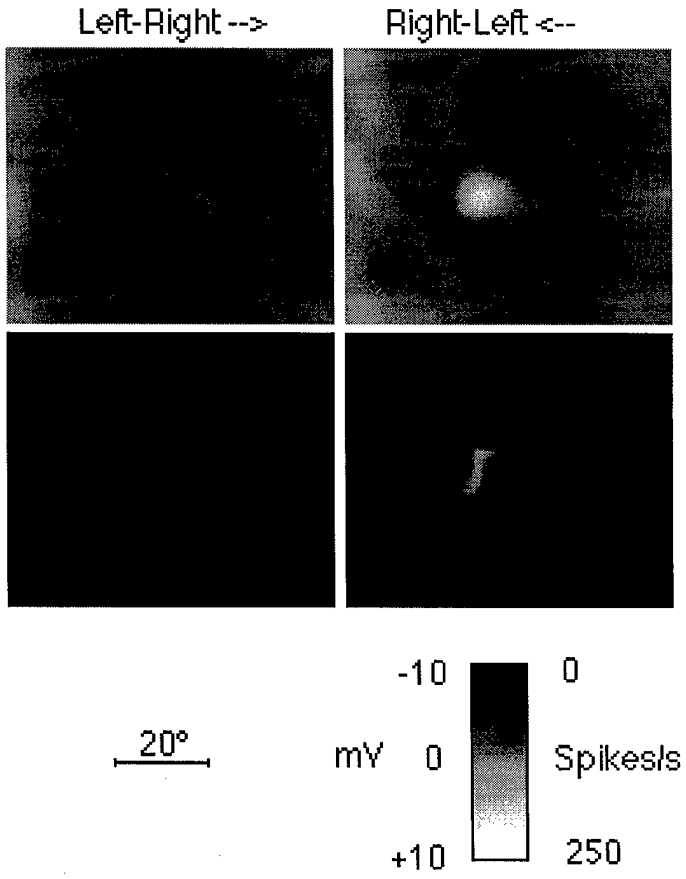

Figure 5: Receptive field plots for an STMD in the hoverfly *Eristalis tenax*.

In each of the plots in Figure 5, the upper panel is the *graded* (sub-threshold) response of the neuron, obtained by digitally filtering out action potentials from each raw response recorded, while the lower plots are averaged firing rates obtained by counting numbers of action potentials generated during stimulus presentation. Because these neurons typically lack spontaneous firing activity, it is only the graded plots that reveal the inhibitory sub-regions of the receptive field, exemplifying the primary advantage of the (technically demanding) single cell intracellular recording technique used. Figure 6 below illustrates similar data, in this case for single passes of a target through the receptive field of a cell.

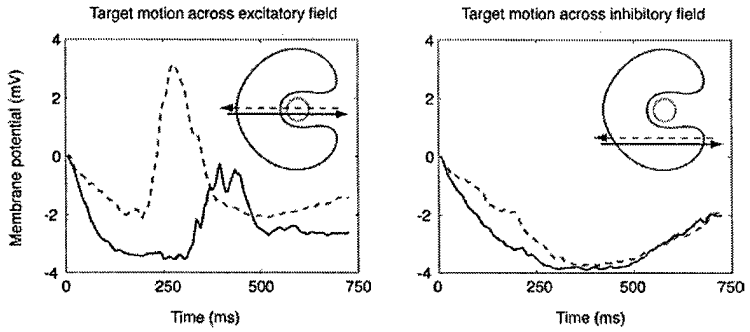

Figure 6: ESTMD responses to moving stimuli aligned with preferred direction, in both directions of motions and different locations within the receptive field.

In the plot at left, the target is drifted left to right (black trace) and then right to left (blue) at the receptive field center of a neuron with the 'notch' on the right hand side. The pictogram in the top right of each figure gives a legend and approximate representation of the receptive field organization, with red outlining an excitatory region, and blue, an inhibitory region. Analyzing the receptive fields of a number of putative ESTMD neurons, we found that the notch in the inhibitory subfield always corresponds to the preferred direction of the ESTMD neuron.

One notable feature seen in plots of the graded membrane potential is that the inhibitory *gain* to small target motion is comparable to the gain of the much smaller excitatory region, producing in some cases up to 8 or even 10mV hyperpolarization. Furthermore, in the neurons illustrated, the central excitatory region, although it shows some apparent response for targets moving in either direction, also shows evidence for at least weak direction selectivity (consistent with the hypothesis that it receives input from EMDs of the Reichardt type), while the inhibitory surround does not. The very high gain in both regions, combined with these other properties suggests a possible basis for selectivity for small targets in the lateral dimension, since a wide variety of other stimuli would inevitably stimulate both excitatory and inhibitory receptive field sub-regions at once, producing weak or absent spiking responses in the output.

3.1.4 The 'Moving Target / Moving Background' Property

With the increasing sophistication of stimulus routines that were developed for the Vision Egg, we were able in the final year of the project to present stimuli that contained small moving targets against moving background patterns. Experiments performed with

such stimuli led to a significant new finding: the capability of some STMD neurons in both dragonflies and hoverflies to discriminate such small moving targets against moving backgrounds, even when the target is otherwise indistinguishable from local features in that background. For brevity, we refer to this capability as the 'moving target / moving background' property.

The best-documented case of this property has been in a cell in *Eristalis* that appears to be a stereotypical neuron that is present from individual to individual. This cell is selective for direction of target travel, and it appears to be capable of detecting small object motion for any combination of relative velocity and contrast that permits target discrimination by the human eye and brain. We were unable find a background pattern that completely abolished its response to the moving target, providing the target continued to move within the receptive field and in the preferred direction. It completely rejects background motion alone.

The following figure illustrates a typical response. In this case, the response was recorded to a control stimulus (blank screen of mean luminance) for 1 second before and after a 2 second period during which both figure and background moved across the receptive field.

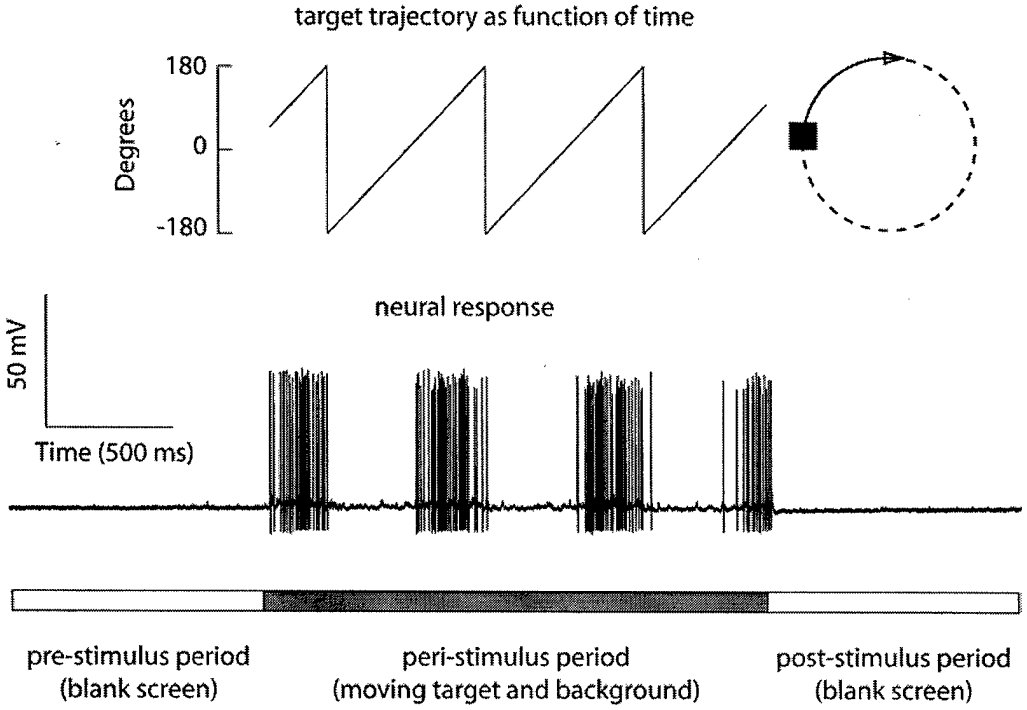

Figure 7: Response by an STMD neuron in *Eristalis* to a small moving target (circular motion) in the presence of moving background clutter.

The background consisted of random texture elements (textels), each subtending approximately one degree in visual space, and distorted onto a cylindrical projection of space around the insect. A target moved against this background in a circular motion, thus coming into and out of phase with *direction* of the background motion, although

there remained a speed differential at all times in this experiment. In the figure shown, the target moved through just less than 4 complete rotations during the peri-stimulus period. The neuron is entirely 'silent' whenever the screen is blank, or background motion is presented alone (not shown). The response pattern includes powerful bursts of action potentials (spikes) whenever the target moves in a specific direction across the receptive field, although the response is weakly inhibited by motion in the opposite direction.

This direction selective response, previously observed in many STMD recordings against blank backgrounds, is evident if the data from a similar recording are re-plotted on polar coordinates. In Figure 8 below, the location of individual spikes recorded during the peri-stimulus period is shown by a colored circle, with a different color for each of the 4 cycles through which the target moves. In each case, spikes were only recorded when the target moves downward. We have recorded other cells in which the response may be to other preferred directions.

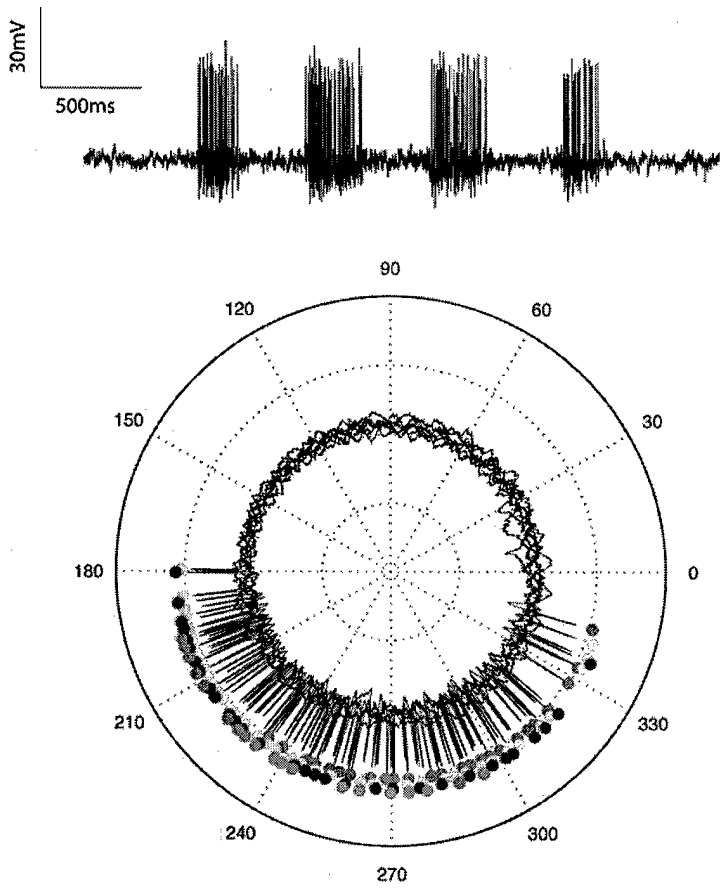

Figure 8: Individual spikes plotted in polar coordinates highlighting direction-selective response. Spikes were only observed when the target was moving downward.

We find that the observed response is extremely robust against the direction or structure of the background optic flow pattern. Only when the target size is similar to the

structure of the background features, of similar contrast and moving at the same speed, in the same direction does the response become completely abolished.

Figure 9 below illustrates the stimulus and response used in Figure 7 above, along with the response to a second stimulus with a higher background contrast. In each case, the pictogram at left shows a screenshot from the actual stimulus sequence. In the high contrast stimulus, the target is smaller and blends almost perfectly into the background of this still frame, while the target in the upper plot is more clearly visible (upper right of the image). During motion, the small target in the high contrast background is visible to human observers, but is much more difficult to make out than the larger target in the low-contrast background. Similarly, the response from the neuron is weaker in case of the small target, although it still shows clear direction selectivity. These results suggest that the individual neurons studied display selectivity for target motion in clutter similar to that found in the human visual system: As a general rule, our observation is that the limits of both systems are similar: if a human can't see the target on the screen, the insect neuron does not fire either.

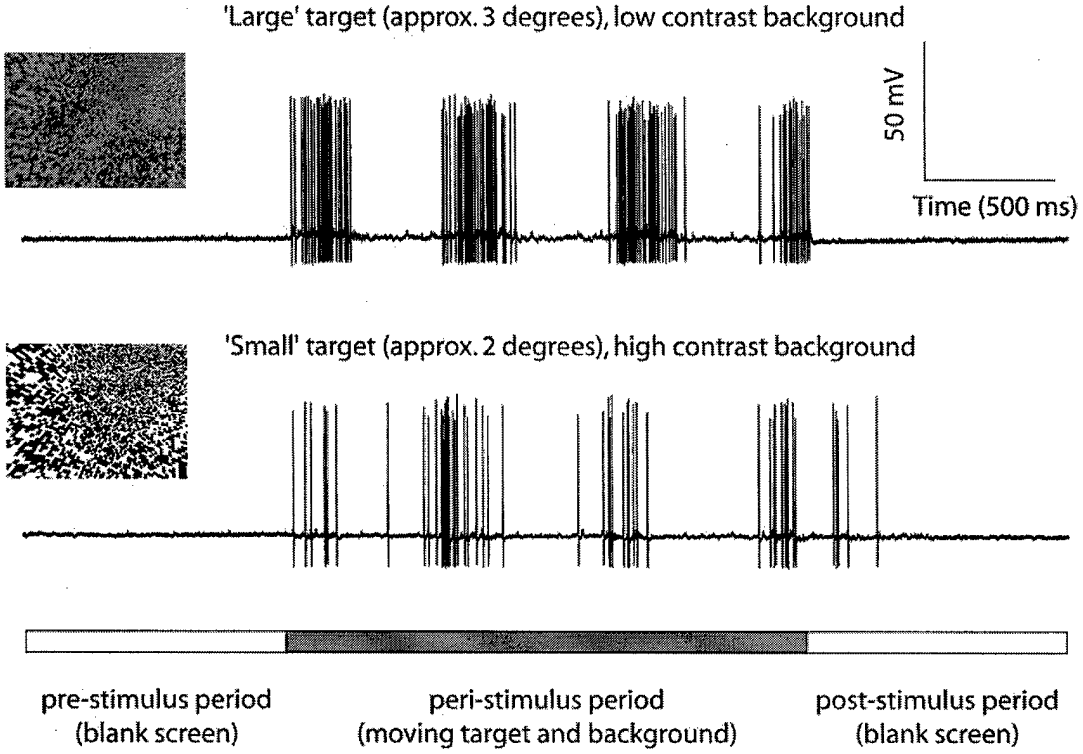

Figure 9: Stimulus and response for a large target and low contrast background (top) and a small target and high contrast background (bottom).

Because it is so difficult to visualize these stimuli in still frame representations, we have constructed movie files depicting them. One such file is included herewith on the CD used for submission of this report.

Because we have on multiple occasions penetrated cells in different specimens of *Eristalis* that have response and receptive field characteristics (including the moving target / moving background property) essentially the same as that reported above, and these cells have all been located in the same area of the lobula, we believe that we have recorded from a stereotypical and identifiable neuron. In the final quarter of this contract, Irene Moyer, a summer student working in our laboratory, has completed a 4 week project to develop these dye filling techniques. We have procured 3 dyes, Lucifer Yellow CH, Cascade Blue and Alexa Fluor 350. We have successfully filled several tangential cells in *Eristalis* with Lucifer Yellow, although not the candidate STMD neuron yet. We are presently trialing a very new dye, Alexa fluor 350, which holds great promise for this work, since the recording properties of electrodes filled with this dye are only slightly worse than electrodes filled with simple electrolyte and much better than with Lucifer Yellow CH (which has been our traditional dye of choice). Alexa also has much higher fluorescence and so promises to be better suited to shorter recordings from smaller cells than anything we have used previously.

3.2 Modeling and Simulation

In our modeling work, we examined a range of processing relevant to STMD responses. During the first half of the project, we focused on the small-field STMD neurons that we putatively labeled ESTMDs, and examined in some detail the responses of elementary motion detectors (EMDs) to small target motion. This led later in the project to concepts for processing that could endow STMD neurons with selectivity for small target size in the direction of motion. Finally, we also examined possible mechanisms for collation of ESTMD outputs, and revised our putative hierarchy of STMD processing in view of the discovery of the 'moving target / moving background' property.

3.2.1 ESTMD Modeling

Study of the characteristics of putative ESTMD neurons led us to propose a conceptual model for how they might operate. The essential features of this concept are: 1) a center-surround receptive field organization with sensitivity to moving objects in the visual field, and, as noted in Section 3.1.3, a small excitatory center and a spatially offset, or 'notched', inhibitory surround; 2) nonlinear dynamic properties, leading to persistence of inhibition or excitation following the passage of a target across a particular point in the receptive field. Inputs to the ESTMD were assumed to be derived from elementary motion detectors.

The particular receptive field characteristics (much as in complex cells in vertebrate visual cortex) are assumed to be formed by competitive integration of excitatory and inhibitory inputs, with a small (ca. 5-10 degree) region in which excitation dominates the response, and a much larger region dominated by inhibition. However, unlike the complex cell, in which the two regions are coaxial, the inhibitory region in the ESTMD is *spatially offset* relative to the excitatory region. The superposition of inhibition and excitation produces the characteristic appearance of a 'horseshoe-shaped' inhibitory surround. We found that phenomenologically, such receptive fields could be modeled well by a difference-of-Gaussians function, in which the negative or inhibitory Gaussian

center is offset in visual space with respect to the positive or excitatory component (see Figure 10 below).

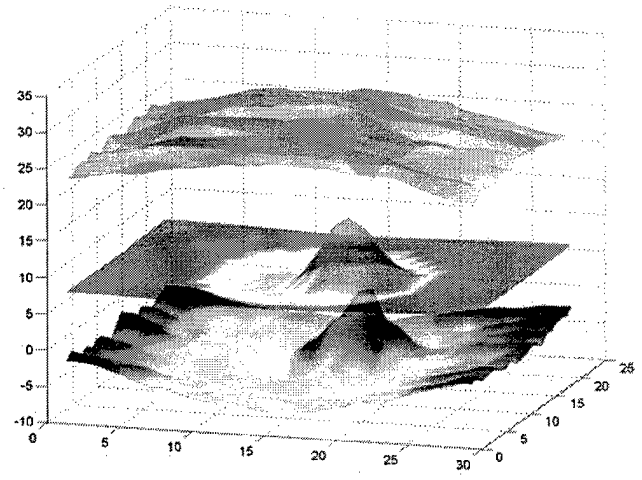

Figure 10: A fit (middle plot) using a difference-of-Gaussians functon, to a typical data set representing an ESTMD receptive field (lower plot). The upper plot is the residual error.

This model is particularly interesting among alternatives because the complex cell model has previously been shown to have widespread applicability to the earliest stages of visual processing ('spatial antagonism' or high pass filtering) in systems as diverse as insect vision and mammalian retinal processing. It is thus plausible to suggest that the neural processing of ESTMDs might have evolved initially from complex cell analogues that operated on EMD outputs to 'sharpen' spatial location of moving features, and which produced, as a consequence, basic selectivity for small targets. Subsequent selection for neural pathways capable of tracking moving targets may have led to the fine-tuning of these receptive fields into the spatially offset fields that we see in our present data.

In this model, the open-ended 'horseshoe' shape of the inhibitory subfield, in combination with the tonic or persistent character of the neural responses, serves several functions. The 'notch' provides a means by which targets moving in the preferred direction can enter the receptive field of the ESTMD without recruiting significant inhibition, whereas motion toward the center from other directions recruits tonic inhibition which depresses excitation as the target crosses the center. Furthermore, motion in the optimal direction recruits tonic excitation that outlasts the passage across the excitatory center. Finally, a visual object whose lateral width is greater than the width of the 'notch' in the inhibitory field would recruit inhibition even if it traveled in the preferred direction. The ESTMD as modeled thus contributes both to the properties of directional tuning and selectivity for laterally small targets.

We suggest that such ESTMDs may be organized retinotopically, with overlapping receptive fields (as in the following diagram, where excitation is shown red, and inhibition in blue, and only a single one-dimensional row is depicted for clarity):

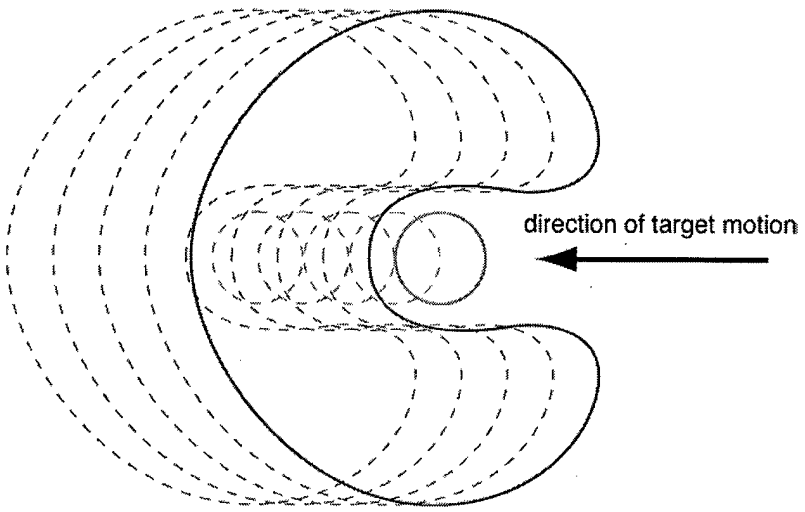

Figure 11: Aligned array of ESTMD receptive fields.

Excitation outlasting the passage of the target across each center of such an array would allow a cumulative build-up of powerful excitation (positive reinforcement) in a post-synaptic collator neuron.

This model makes several clear predictions:

1. If we record responses to targets drifting across the excitatory center, in both the preferred and anti-preferred directions, delayed excitation should lead to asymmetry in the strength of the response to target motion as it crosses the inhibitory 'flank' of the ESTMD, even though the flank itself is not inherently direction selective. This hypothesis has been tested and verified experimentally by results like that shown in Figure 6 in Section 3.1.3. In that figure, excitation by preferred direction target motion outlasts the relatively brief crossing of the excitatory center and limits inhibition by the left-most inhibitory part of the receptive field to negative potentials considerably smaller in magnitue than those elicited by a crossing of the same inhibitory region in the opppsite direction.
2. The asymmetry in inhibitory gain should disappear if we were to repeat the experiment with the target appearing within a limited portion of the receptive field, e.g., if it moves only within the inhibitory subfield (thus altering the recent stimulus history).
3. This model predicts a long response latency in the ESTMD and in downstream STMDs, due to the tonic nature of the response (a form of non-linear low-pass filtering) and the positive reinforcement produced by targets crossing sequential receptive field of ESTMDs. As noted earlier, the typical latency in response of STMD neurons is much longer than that of other insect tangential neurons - of the order of 40-50 ms, compared with 12 ms in an HS neuron (wide-field movement detector).

4. A final prediction is that delayed inhibition and excitation within the ESTMD would alter the velocity tuning of a collator (STMD) cell radically compared with that of a simple EMD collator like an HS neuron. Although it is premature to attribute this difference to the kinetics of ESTMD receptive field interactions, this seems a likely source.

In considering how such an ESTMD might be implemented physically, we sought a model that is: both neurobologically plausible, and a reasonable a basis for an artificial circuit analog; consistent with a retinotopic distribution; and in some sense based on a minimally complex architecture. Such a physical model is illustrated below in Figure 12, in a one-dimensional example for sake of clarity:

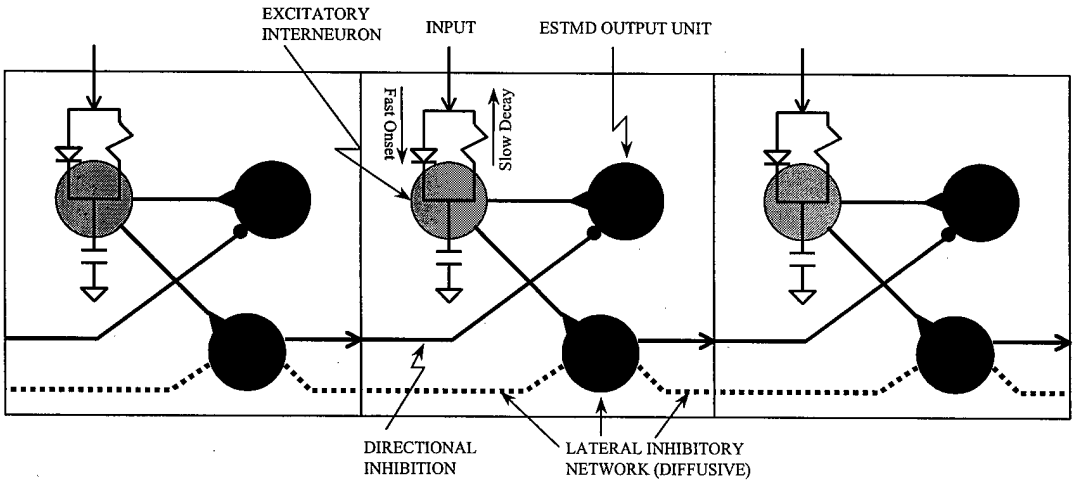

Figure 12: ESTMD architecture (one-dimensional array for illustration).

Two major simplifying assumptions are made in this model: one, the temporal characteristics are attributed to a single 'excitatory interneuron' per ESTMD unit cell, and two, only local interconnections are made between ESTMD units (although signals can propagate over larger distances by diffusion). The dynamic characteristics of the 'excitatory interneuron' comprise a fast onset and slow decay of excitation due to input from peripheral stages in the visual motion pathway. This 'interneuron' directly excites an ESTMD output unit, and also provides input to a diffusive network that is used to propagate inhibition. (This arrangement eliminates the need for two time-dependent units, one for excitation and one for inhibition.) Although signal propagation between inhibitory units is diffusive, these units actively inhibit neighboring output units in a directional fashion: in the one-dimensional example of Figure 12, inhibition is propagated from an inhibitory neuron onto the output unit to its right, but not the one to its left. This particular architecture is therefore tuned to leftward motion. The same diffusive network could be used to form ESTMDs with other directional tunings, by virtue of different patterns of active inhibitory connections onto different output units.

Although the example above is one-dimensional, we simulated ESTMDs arranged in two-dimensional hexagonal retinotopic arrays, in an architecture in which active inhibition impinges on an ESTMD output unit from five out of six nearest neighbors. The

preferred direction for excitation is thus the direction from which active inhibition does not impinge on the ESTMD unit. (A stimulus moving in that direction does cause some initial inhibition due to diffusive propagation to neighboring cells that do have inhibitory connections to the target cell). Although excitatory receptive fields of ESTMDs are typically several ommatidia wide in visual space, we modeled each ESTMDs with a single excitatory input. Thus our models could be thought of as either a 'spatially compressed' ESTMD, or as operating on summed input signals from a number of adjacent EMDs.

A 61-unit hexagonal array of ESTMD cells was selected for simulation, and ultimately for implementation in analog silicon. Simulations were performed using the tool SPICE. The temporal properties were based on the response of a nonlinear circuit (described in detail in Section 3.3.2 below) with rapid charge and slow discharge characteristics. The diffusive network was modeled with a resistive grid, in which the spreading or space constant is determined by the ratio of shunt to lateral resistances (actually implemented with active devices). Inputs were assumed to constitute moving pulses corresponding to the retinotopic output of earlier stages of motion processing, as induced by passage of a small moving target. With appropriately chosen scaling of inhibition and excitation, responses such as that depicted below in Figure 13 were obtained from these simulations.

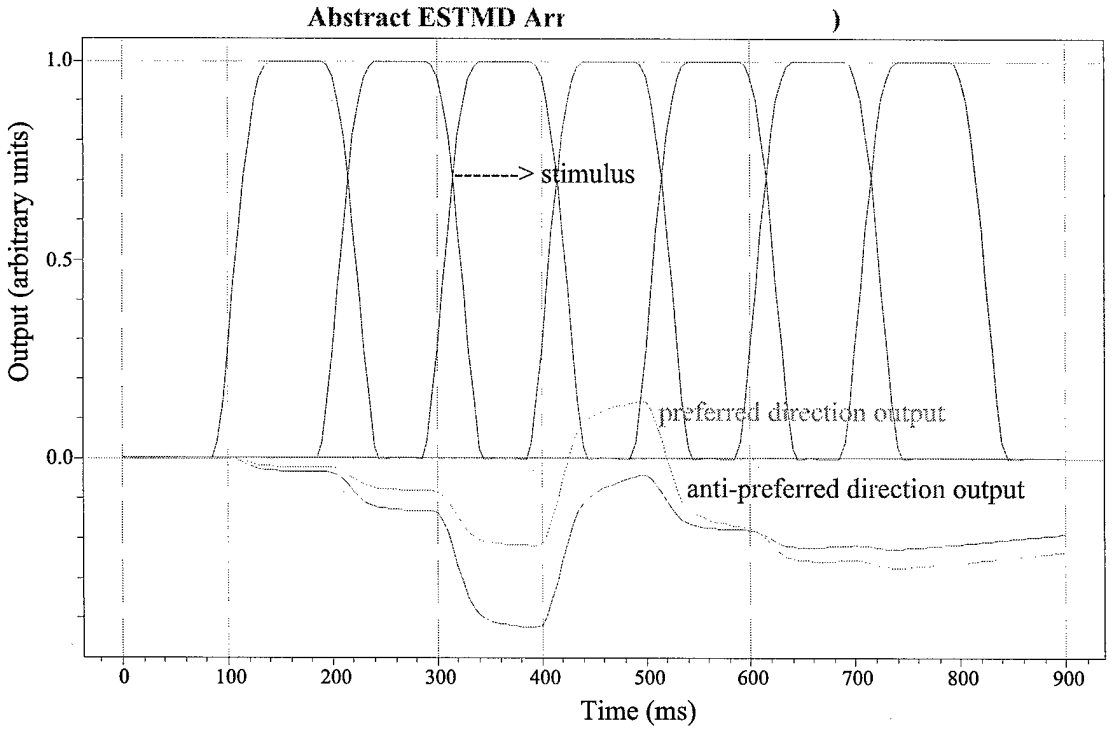

Figure 13: Abstract ESTMD array response to a 'moving target' crossing the excitatory center, in both the preferred (green) and opposite or antipreferred (red) directions.

These responses may be compared to the actual data taken from an ESTMD neuron, in the left-side panel of Figure 6.

3.2.2 Selectivity for Longitudinally Small Targets

During our simulation studies, one topic that we investigated was the response to small moving targets of the elementary motion detector itself, the presumed front-end for small-target detection. These efforts ultimately led to a model for selectivity for smallness of a moving visual object in the longitudinal dimension (direction of travel).

This model was built upon observations of how EMD responses to moving targets depend on the characteristics of temporal filtering that is assumed to take place in early vision. Basic correlational EMDs were simulated, with inputs constituting moving targets with constant contrast with background, and of various longitudinal extents. We found that when the early vision 'prefiltering' passes a DC component (as with a lowpass filter) the EMD response becomes triphasic as the target extent becomes small. Prefiltering that passes no DC (such as a bandpass filter) does not result in such triphasic EMD outputs. This is illustrated below in Figure 14, which shows the response of an EMD to targets of four different sizes moving across its receptive field, for filters of each type:

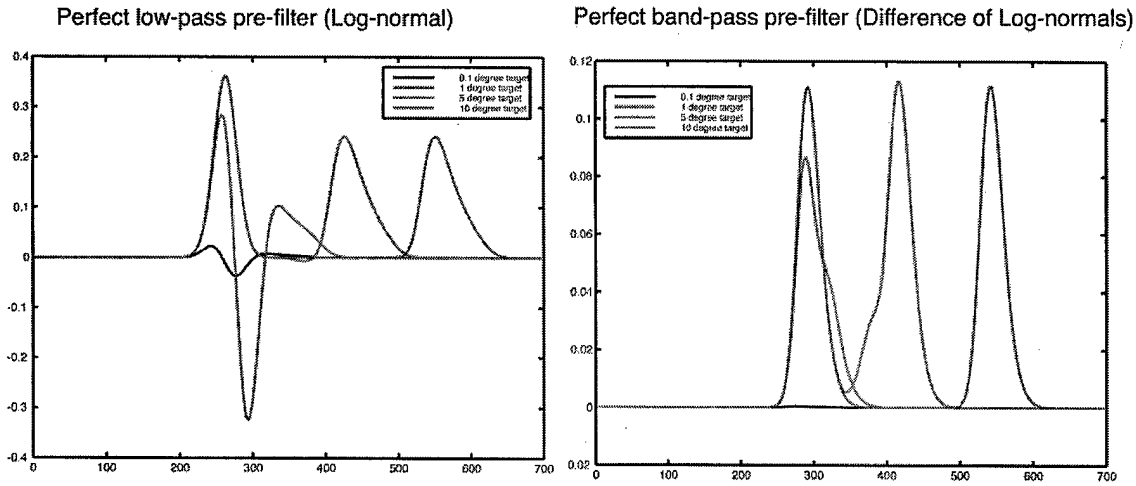

Figure 14: Response of a correlational EMD to passage of a moving target of different longitudinal extents. Left response is with lowpass temporal prefiltering, and right, with bandpass temporal prefiltering. Abscissa is time in ms and ordinate, EMD output in arbitrary units. Target speed is 40°/s. The 'perfect low-pass', filter used a log-normal impulse response with 10ms time to peak and sigma=0.4. 'Perfect band-pass' used a difference of this (gain unity) and a second log-normal with the same sigma but 30ms time to peak, resulting in an impulse response with zero mean. Longitudinal target extent is a parameter in each case.

This model used 1 degree inter-receptor angle, 1.4 degree (half-width) Gaussian blur (2 dimensions), 100 ms pre-stimulus period (no target motion), dark target (luminance 0) on a bright background (1.0), with a first-order (exponential) delay filter (time constant=35 ms). The 'double log normal' impulses responses used for the prefilters have

been previously shown to give excellent fits to first order kernels measured in fly lamina monopolar cells (LMCs) with white-noise techniques]. The LMCs are likely presynaptic elements to the EMDs, and their responses reflect both their own highpass dynamic characteristics and the lognormal lowpass characteristic of the photoreceptors which supply their inputs.

LMCs, however, are actually 'imperfect' high pass filters, which typically transmit a weak DC response, and indeed become strictly low-pass at lower light levels. To model this feature, we altered the weight of the high pass component of the double lognormal, which generates impulse responses with small negative or positive means, and in the frequency domain leads to passage of small inverted or noninverted DC components, respectively. Figure 15 below shows model outputs for 'imbalanced' bandpass filters based on this imperfect LMC highpass characteristic:

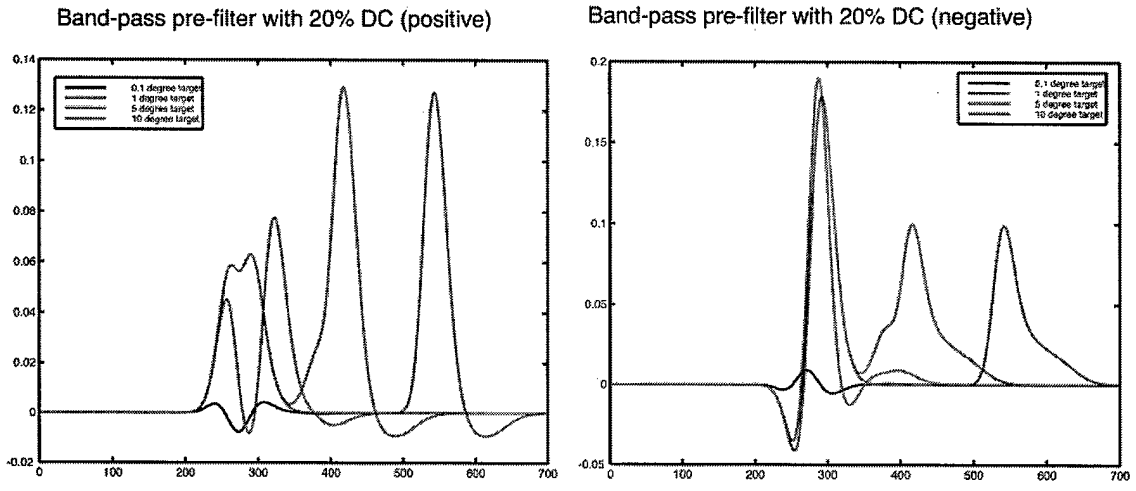

Figure 15: Response of a correlational EMD to passage of a moving target of different longitudinal extents. Left response is with bandpass temporal prefiltering that passes 20% noninverted DC, and right, with bandpass temporal prefiltering that passes 20% inverted DC. Other parameters as in Figure 14.

In these two 'imperfect' variants, the second log normal part of the impulse function was given a gain of either 0.8 or 1.2 before differencing, yielding either a positive or negative mean (and thus DC component).

The modeling suggests that if EMD prefilters pass a significant amount of DC, outputs may go both above and below zero. Importantly, however, we see negative-going transients primarily for small targets moving at lower speeds: much longer targets produce positive responses only, as they cross the receptive field, independent of the model pre-filter that we select. The signal arises from a quasi 'wave interference' process whereby the residual impulse response elicited by the leading edge of the target is overlapped with the early part of the impulse response elicited from the trailing edge of the target. A filtering strategy that is selective for the negative-going transients in such responses might yield a huge gain in response selectivity for small targets. A major

advantage of such a strategy is that it could be applied even prior to higher-order small target detectors such as the ESTMD in order to obtain a selectivity for events consistent with the passage of a longitudinally small target.

We developed a detection algorithm employing this strategy, which is based on taking the product of the integral of the mean output response of an EMD, with the mean integral value of the rectified transient signal having an opposite polarity. This algorithm was shown to be effective and unambiguous in simulations. Results of such simulations are shown in Figure 16 below, in which several quantities are plotted as functions of the target width and target speed. Panel A shows the time averaged (mean) output of the 'raw' (low-pass pre-filtered) EMD array. As expected, this is not selective for small targets, and shows sharpest tuning for target speed when target size is smaller. Panel B shows the time-averaged output of EMDs after half-wave rectification of the negative-going transient responses. As described above, these are most prominent for small targets moving at lower speeds. While such outputs in themselves might give an indication that a feature is a potential target, it is important to note that this is inadequate as a model for target selectivity in its own right, since targets moving in the opposite direction will give inverted responses and thus produce output of such a model with similar tuning to that in panel A. In panel C, however, we have 'gated' the half-wave rectified signal with the mean output, which is in itself direction selective. This provides a promising strategy that is selective for longitudinally small image features, while retaining the direction selectivity inherent to EMDs.

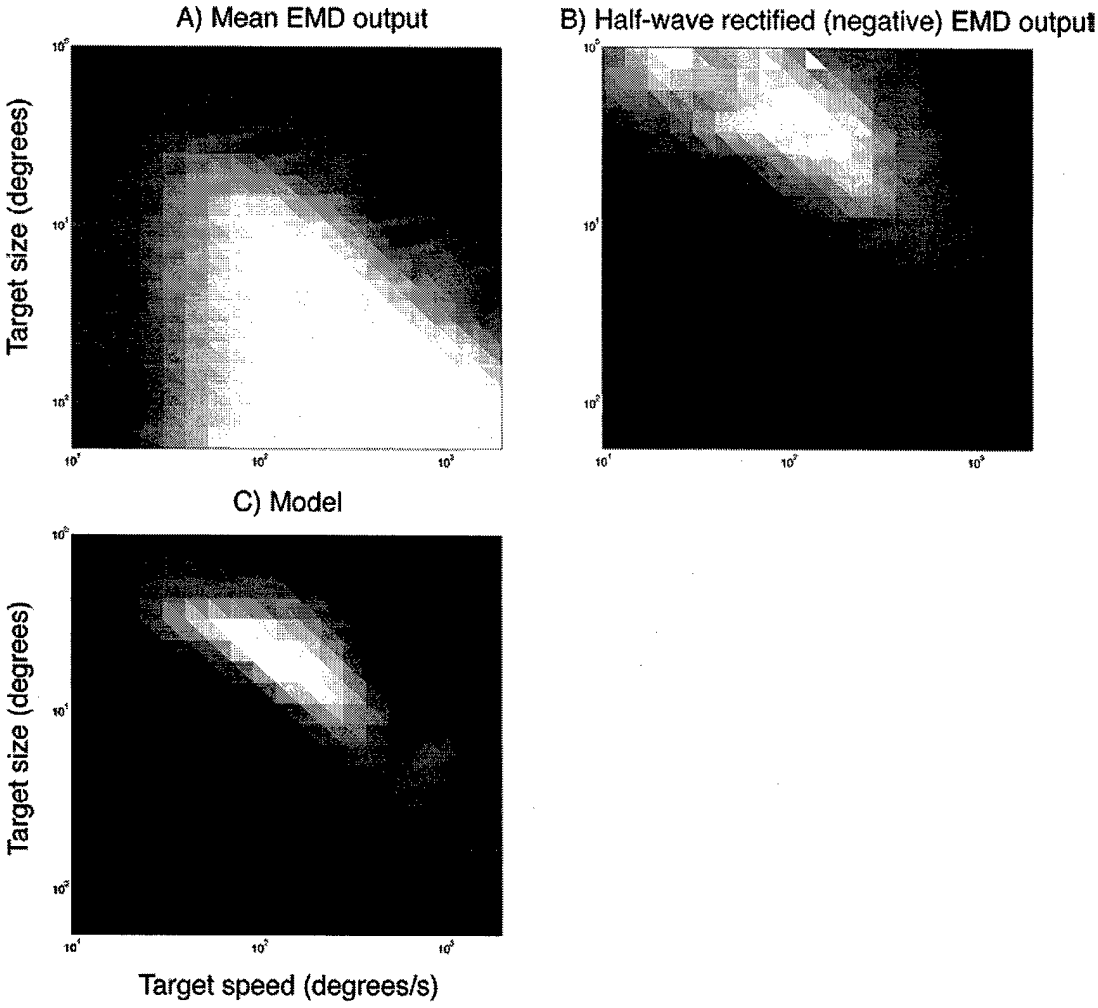

Figure 16: Making use of the characteristic response of EMD (with lowpass prefiltering) to longitudinally small moving targets: a simple second-order motion processing model with selectivity for small targets and direction of motion. A) is the time-averaged EMD output, B) the time average of negative half-wave rectification, and C) the average model output, all as functions of target size and speed. Brighter colors in the false-color images indicated larger values.

Note the consistency of the results shown in Figure 16C with the STMD responses in the left panel of Figure 4: The optimum response shifts to higher target speeds as target size increases.

Finally, we note that this model represents a particular case of a general approach to filtering EMD outputs for events consistent with the passage of longitudinally small visual objects: that is, 'looking for' features in the EMD output that are particular to such events. The presence of a triphasic response is an especially distinctive feature, but others might also be useful. For example, in the case in which perfect bandpass filtering precedes the EMD, then a bimodal response that remains well above zero between the peaks might be taken as an indication of small target passage. Also, although we have

implemented the processing here by a non-linear operation (rectification) there are alternative and equally plausible (in the biological sense) strategies (e.g. linear wavelet filtering) that could be used to extract the same temporal response 'features'.

3.2.3 Final Status of STMD Modeling

Based on the results of the neurobiologcal and modeling efforts undertaken during the project, we now posit the following major functional elements for small target processing, leading to wide-field STMD capability:

1. Elementary motion detector (EMD): The correlational EMD or its constituent parts (i.e., correlator units) are still regarded as the likely front-end processing for STMD neurons. Evidence is indirect, but there have been no findings yet to contradict this supposition.
2. Longitudinal target size discrimination: Ability to discriminate 'smallness' of target in direction of motion. The relevant modeling reported in Section 3.2.2 is consistent with the experimental results exemplified by Figure 4 in Section 3.1.2. Such processing may serve to 'prefilter' the outputs of EMDs for events consistent with passage of a small object.
3. Target / background speed discrimination: This is an essential capability needed to distinguish a moving target from a moving cluttered background (which may contain small features indistinguishable from 'targets'). Some initial efforts at modeling this capability in abstract (SPICE) simulations were conducted under support of Navy SBIR contract N00014-03-M-0171. This approach involves a comparison of the traversal times across pairs of ommatidia of 'small target events' with the expected traversal times for moving background (which might well have features like small targets). This comparison is achieved with an EMD-like element that is tunable by feedback representing state of local background motion, and which performs anticorrelations rather than correlations so that it is responsive to events inconsistent with that motion.
4. Lateral target size discrimination: Ability to discriminate 'smallness' of target perpendicular to direction of motion. This (along with enhancement of directional selectivity) may be a principal function of cells that we have labeled ESTMDs as a result of work on this project.
5. 'Dendritic processing': A mechanism in a wide-field collator cell for stimulus summation and artifact rejection. Reinforcement of either active or diffusive potentials along a dendrite is presumed to occur by sequential excitement of ESTMDs along continuous tracks in visual space. This feature exploits the constraint of continuity of motion to obtain higher-confidence detection of a moving target. Although not modeled in simulations, this capability was modeled in silicon as detailed below in Section 3.3.4.

3.3 Silicon Modeling: Circuit Designs and Results

3.3.1 Transistor and Basic Test Structures

The transistor test structures and other small test circuits placed on the test chips described in Section 2.3.1 were intended to allow evaluation of basic characteristics that impact larger circuits implementing STMD models (and in fact in many cases, analog neuromorphic designs in general). Perhaps the most important of these is matching of device properties from transistor to transistor, which affects signal accuracy and the ability to set reference levels in virtually every circuit design considered. Also of interest were leakage currents (affecting the magnitude of time constants obtainable in dynamic circuits), subthreshold behavior, and functionality of novel devices fabricated in silicon-on-sapphire.

Results from the Agilent 0.5μm bulk CMOS process (used for ***chip_1_bulk***) suggested that it is very well-controlled, with good device matching and extremely low leakage currents. Current mismatches among inside pairs of 5μm square devices were generally well under 10%, with standard deviations of the extracted threshold difference being less than 3mV for PMOS and less than 2mV for NMOS, on a sample size of eight chips. Smaller samples were evaluated for 2.3μm square and 8μm square devices, so these results are less definitive, but the matching of the larger transistors appears to be consistent with the generic model (standard deviations varying inversely with the square root of device area). The smaller transistors, however, display poorer matching than would be expected from results on the larger devices, suggesting that the lithographic limits and other second-order factors may be influencing their characteristics.

Additionally, common centroid quads with total device area of $25\mu m^2$ were tested for comparison with the individual square devices. Device matching for the common centroid geometry, when amortized by area of the entire layout, is about 20% better for n-channels and no better for p-channels, relative to square devices. Given the impact of the common centroid approach on complexity and routing, we concluded that simple matched pairs would be the layout technique of choice. Unfortunately, loss of access to the Agilent process precluded further circuit development in this process.

Testing of individual transistors on ***STMD_chip***, fabricated in TSMC 0.35μm mixed-signal bulk CMOS, showed somewhat poorer matching than for devices of comparable size fabricated in the Agilent 0.5μm process, particularly for p-channel devices. The devices tested were 4.8μm square and were arranged in matched inside pairs. Standard deviation of NMOS threshold variations was on the order of 5-6mV, but was 8-9mV for PMOS. This may necessitate the use of larger PMOS devices for design, or (more likely) doubling up of transistors (use of dual pairs) in match-critical circuit applications. In addition, tests of dynamic circuits suggested larger leakage currents than in the Agilent process, probably limiting time constants to less than 1s.

Device matching on the SOS chips (the gratis chip and ***chip_1_sos***) gave evidence of poorer matching than either bulk process. For NMOS, the standard deviation of threshold variations was found on the order of 6mV for 5μm square devices on the gratis chip, but this result excludes a significant number of outliers in the sample with mismatches larger than 50mV (a value that renders them useless for analog design purposes). Threshold

mismatches were somewhat smaller as expected for 8μm square devices on ***chip_1_sos***, but the statistics were questionable due to the continued presence of outliers with very large mismatches. PMOS on ***chip_1_sos*** (8μm square devices) gave standard deviations of about 3.5mV. Lightly doped MOS transistors, as expected, gave improved matching performance, particularly for NMOS devices.

Because the n-channel transistors in this process are particularly susceptible to floating body effects (commonly manifest in the "kink effect," a reduction in drain resistance in saturation), we speculated that the large mismatches may actually arise from the floating body rather than the channel interface. (This speculation was confirmed by results from devices with body connections that were fabricated and evaluated under support of another project. However, layout of devices with compact body connections requires violation of existing design rules, and makes verification difficult if not impossible.)

Test results from lateral bipolar junction transistors on the SOS chips were generally negative. Ungated devices showed evidence of high collector-emitter conductivity and little transistor action, suggesting that the source-drain block is not entirely effective at the small base width geometries needed for reasonable current gains. The gated devices showed transistor action, although at higher currents the slope of the V_B / I_C relationship was considerably smaller than the inverse thermal voltage, suggesting series resistance or other nonidealities at work. Current gains were reasonable for the gated npn devices (10-30 at 1μA collector currents, higher at nA level currents), but for the pnp devices were considerable poorer (current gains from less than unity to three). Leakage currents at low base voltages were substantial in the npn devices (not surprising since the vendor now recommends a minimum gate length of 0.8μm for their regular NMOS devices due to leakage concerns). Additionally, device matching among the BJTs appeared to be no better than that of MOSFETs. Our conclusions were that lateral BJTs would not be generally useful.

Depletion mode devices fabricated in SOS functioned as expected. No statistics were taken for device matching in these transistors.

Results on primitive devices in the SOS process were significant in convincing us that further development should be pursued in bulk silicon.

3.3.2 Log-Domain Filter Circuit

During the course of the project, a novel methodology for the implementation of long time-constant log-domain filter circuits was devised and developed. The concept is described in detail in a manuscript prepared for publication and previously passed to the contracting officer's representative; we describe the fundamentals of this circuit and its development here for completeness.

A schematic diagram of the basic circuit is depicted in Figure 17:

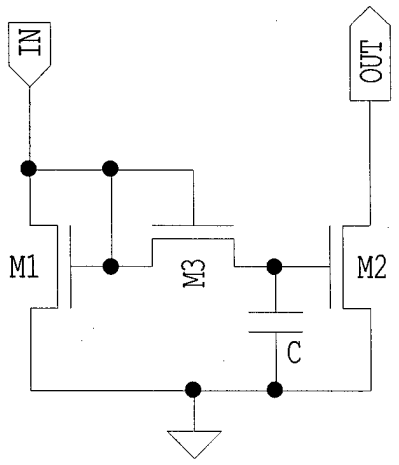

Figure 17: Basic log-domain filter circuit.

The circuit is operated in the subthreshold regime, and takes advantage of the fact the 'resistive' element M3 has an exponential current-voltage relationship similar to the current mirror devices M1 and M2. The input and output are both unipolar current signals. Under idealized assumptions regarding the transistors in the circuit (absence of junction leakage and body effect, and drain current independence of drain voltage in saturation), it can be shown that the input-output relation may be written:

$$(1 + CU_T / I_{0R}\, d/dt) I_o = I_i ,$$

where the input and output transistors M1 and M2 are assumed matched, I_{0R} is the specific current parameter for M3, and where U_T represents the thermal voltage. I_i and I_o represent the input and output currents (the drain currents of M1 and M2, respectively). The circuit thus implements a linear first-order lowpass filter (a real pole) in the current domain, with time constant $\tau = CU_T / I_{0R}$.

Two of the assumptions made regarding the idealized circuit are effectively true when it is fabricated in silicon-on-sapphire: there is no junction leakage, due to dielectric isolation of the individual devices, and although the body effect is present, it does not significantly affect external linearity of the circuit, due to the 'floating substrates' of the transistors. Both of these assumptions, however, are not valid for bulk silicon and have significant implications for circuit performance. The most serious of these is dependence of the time constant on mean current levels. The third assumption, independence of drain current from drain voltage, can be made approximately true in either SOS or bulk silicon by the use of long-channel devices.

Simple modifications to this circuit allow electrical controllability of its time constant. These involve level-shifting the gate of the device acting as a nonlinear resistor (M3 in Figure 17) with a follower transistor as illustrated in Figure 18 below:

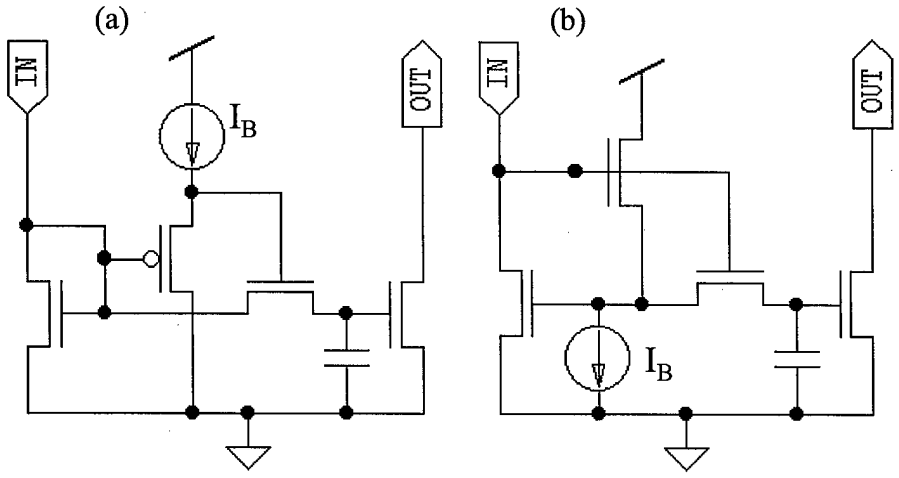

Figure 18: First-order lowpass filters with level-shifting followers to modify time constant. In (a) the gate voltage of the nonlinear resistor device is shifted by a follower transistor of the opposite type. In (b), it is shifted by connecting it to the gate of a follower/buffer of the same type.

In the circuits of Figure 18, the level-shift voltage, and thus the time constant, is controlled via the follower bias current I_B. The operation of these circuits is, however, restricted by bandwidth requirements on the follower circuits in them.

One reason that this circuit is of interest for this project is that it provides a means to model the nonlinear, rapid-activation, slow-decay characteristics that are reflected in the 'tonic' ESTMD response. When input and output current levels are increased from weak inversion to moderate or strong inversion levels, then the charging and discharging behavior of the filter becomes asymmetric. When operated in strong inversion, it can be shown that the nonlinear filter transfer characteristic takes the form (using the Heaviside notation)

$$I_{OUT} = \left(\frac{KU_T^{\,2}}{2}\right) \ln^2\left[\frac{1}{(1+\tau\, d/dt)} \exp\left(\frac{\sqrt{2I_{IN}}}{\sqrt{K}U_T}\right)\right],$$

where I_{IN} and I_{OUT} are the input and output currents, respectively, K is the transfer constant (in A/V^2) of the input and output transistors, τ is the time constant of the filter, and U_T is the thermal voltage. (This assumes that the transistor serving as a nonlinear resistor in the circuit remains in weak inversion, as would be the case for all but extremely large and rapid excursions of the input). Simulated temporal response of the filter to a square wave input when operated in the moderate to strong inversion regions is depicted below in Figure 19:

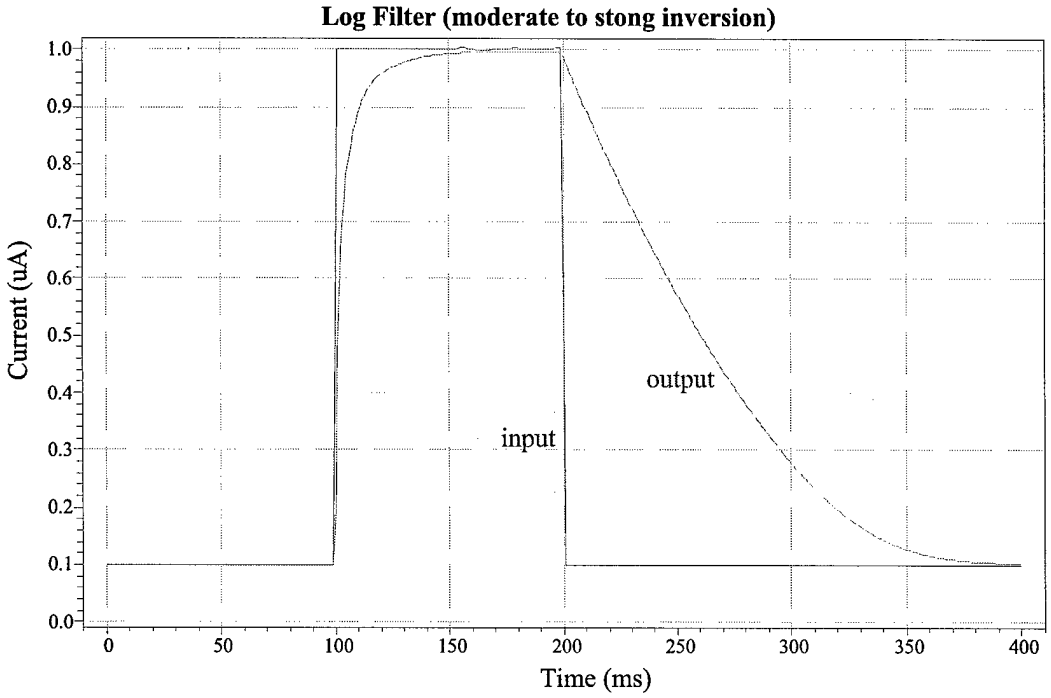

Figure 19: Log domain filter response when operated in moderate to strong inversion.

Similar nonlinear characteristics, with even more pronounced asymmetry between charge and discharge, can be obtained with cascoded circuits to be discussed below.

The basic circuit of Figure 17, when fabricated in SOS, gave generally positive results. The n-channel version showed some nonlinearity in subthreshold (pseudolinear) operation, but the linearity of the p-channel version was good (total harmonic distortion on the order of 3% was measured at the –3dB point in experiments with sinusoidal inputs). Natural time constants were on the order of hundreds of milliseconds (reflecting relatively high channel leakage in the SOS devices). In the version of the circuit with electrical control of the time constant, the use of a low-doped n-channel follower permitted a practical variation of that time constant over a five-decade range.

When the filter circuit was operated with the input and output devices in moderate to strong inversion, it displayed the expected rapid charge / slow discharge characteristic. Figure 20 below shows an example of data obtained from a p-channel SOS circuit (version with electrical time constant control), in response to a square wave input. Due to the polarity of the circuit and the buffer amplifiers used for interface, increments are represented by negative excursions and decrements by positive excursions in the input and output traces. The circuit time constant was set arbitrarily to show the disparity between charging and discharging, at the given input frequency (500Hz).

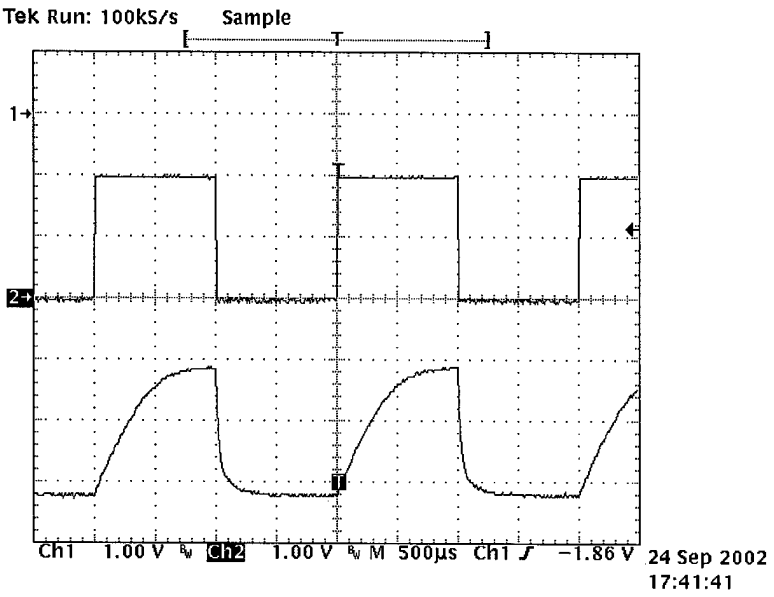

Figure 20: Operation of the p-channel SOS log domain filter in moderate to strong inversion. Top (trace 1) is the square wave input and bottom (trace 2) is the circuit output. The effective vertical scale is 0.5µA per division. Increasing current is in the downward direction for the ordinate.

When fabricated in the Agilent 0.5µm bulk CMOS process, the basic log-domain filter circuit (both NMOS and PMOS versions) was untestable due to the magnitude of the time constants, reflecting extremely low channel and junction leakage currents in this process. Only an NMOS version with a level-shifting follower proved testable, and it showed good performance and linearity, although corner frequencies higher than a few hundred mHz could not be obtained. However, it also showed evidence of the significant negative impact of the body effect in bulk silicon: dependence of the circuit time constant on mean filter state. When the circuit is operated in the nonlinear 'tonic' regime, this results in less difference between the fast time course of excitation and the slow post-excitatory discharge, than in the same circuit without the body effect (e.g., as implemented in SOS), in addition to rendering the temporal characteristics dependent on the mean input current.

A solution to this problem was developed under joint support of this contract and US Air Force SBIR Contract F08630-02-C-0013. By using a follower transistor of the same type as the filter for electrical control of the time constant, the body effect in the follower can be used to cancel the body effect in the main filter itself. This configuration is made possible by placing the follower in a separate well, which is biased below the positive supply, in order to promote the follower circuit bandwidth well beyond that of the filter proper.

In addition, a new approach to obtaining the 'tonic' nonlinear behavior was developed. The 'tonic' property was originally obtained by applying above-threshold currents, resulting in a sub-exponential current-voltage characteristic in the input and output devices, and breaking the pseudolinearity of the circuit. This has the disadvantage of requiring at least microampere-level currents at every cell in an array. However, the

same effect can be obtained by using cascode devices to force a sub-exponential current-voltage characteristic. This allows the circuit to be operated in the tonic mode even in the subthreshold regime, and converts it back to a micro-power circuit.

The filter design used on the final chip, fabricated in the TSMC 0.35μm bulk CMOS process, is depicted in schematic form in Figure 21 below:

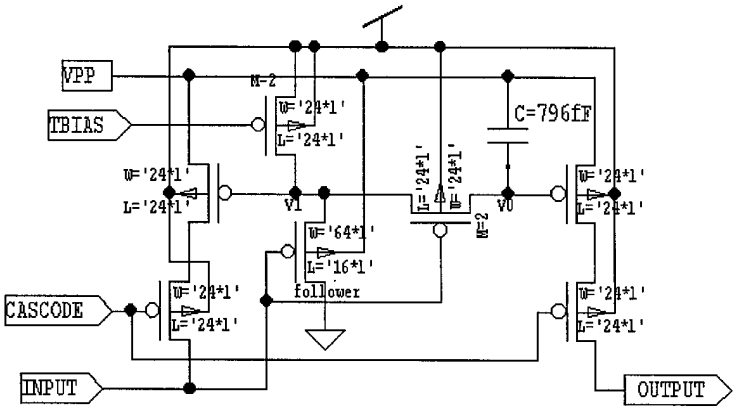

Figure 21: "Tonic' filter implementation. The VPP port represents an additional power supply terminal that is supposed to be held at a potential at least several hundred millivolts below the positive supply (VDD). The transistor labeled 'follower' is situated in a separate n-well that is maintained at VPP rather than VDD. The transistors with gates connected to CASCODE, when properly biased, force a sub-exponential current-voltage characteristic on the input and output stages.

Functional tests showed that this circuit works well in both the pseudolinear and 'tonic' regimes. Data were included in the manuscript submitted for publication.

3.3.3 ESTMD Model Arrays

Analogs of ESTMDs were included on all test chips fabricated during the project. The general architecture of the unit STMD cell is illustrated (in this case, for the final version implemented in bulk silicon on ESTMD_chip) in Figure 22:

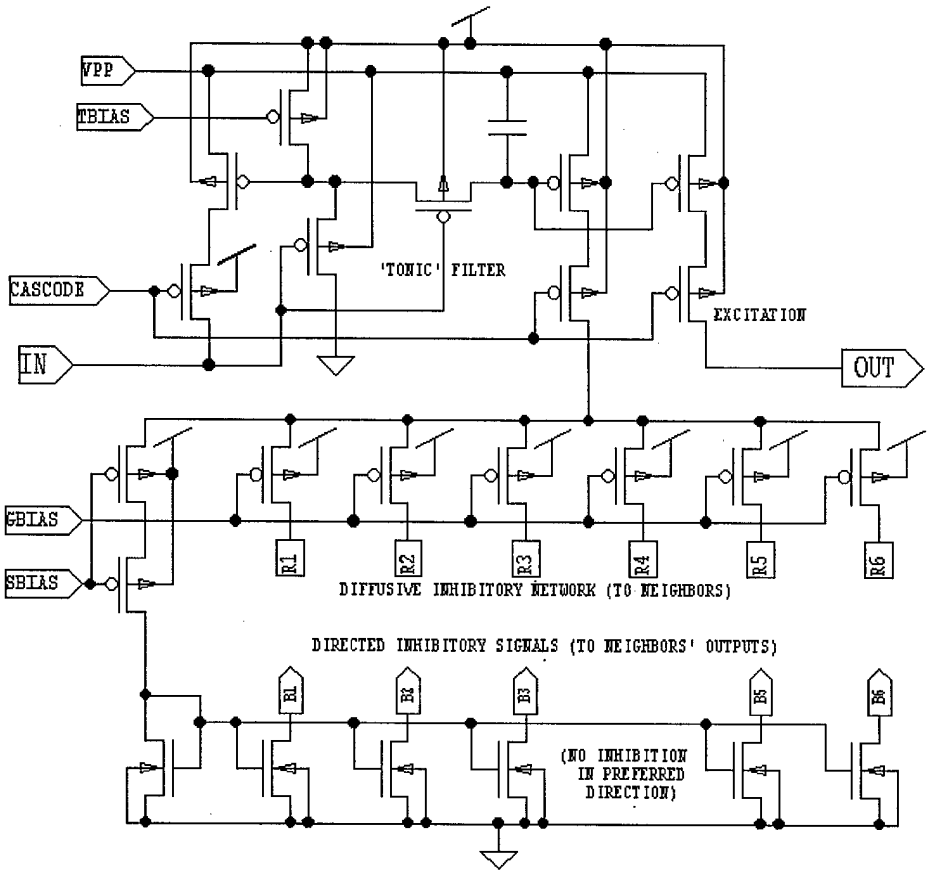

Figure 22: Architecture of the unit ESTMD cell on *ESTMD_chip*. VPP is the independent well bias discussed in the text. The bias applied at TNBIAS determines the time constant of the 'tonic' filter, and the CASCODE bias is used to force a subexponential characteristic on the input and output of the filter. The potential difference between GBIAS and SBIAS determines the space constant for the spread of diffusive inhibitory signals. All biases are global in an array of ESTMDs. In this circuit, direction 4 (downward in the array) is the preferred direction, due to the absence of a directed inhibitory signal in that direction.

ESTMD unit cells were arranged in hexagonal arrays in test structures on each of the fabrcated test chips. Only local interconnections to six nearest neighbors are made by each cell in this array. A diffusive network is used to propagate inhibition. In each array, the central 37 cells were addressable one at a time for input, and the output of the single cell at the center was brought out for observation. The array was stimulated during testing using a "single pixel" stimulus without directional properties, and of a fixed amplitude, which was steered across the array in a particular direction by applying a sequence of addresses. Thus the model represents a 'spatially compressed' version of a biological ESTMD, with input preprocessing resulting in a stereotyical pulse input in response to a 'small moving target event.'

In these arrays, the relative scaling of inhibition and excitation is important in order to obtain a net excitatory response to stimuli moving in the preferred direction, and net

inhibition in other directions. This scaling is accomplished by the sizing of transistors in the circuit. In our initial design efforts, full transistor-level simulations of the array were used to determine appropriate device sizing, but these simulations proved problematic with regard to convergence. Ultimately, some results were obtained and used to determine relative scaling of inhibitory and excitatory signals in the SOS implementation on ***chip_1_sos***, although there was evidence of numerical problems. For subsequent design efforts (for ***chip_1_bulk*** and ***ESTMD_chip***) we developed a version of the array with abstract elements, which still retained the first-order characteristics of the circuit model, but for which convergence was improved.

Test results on the SOS array validated the general principle of the ESTMD design, although improper current scaling was evident. Figure 23 shows the time-course of the output of the central EMD cell in the array, for five different 'stimulus paths' across its receptive field. These are arranged in the order of the level of excitation they elicit, from the initial path, which does not cross the excitatory region at all, to the final path, which crosses the excitatory region in the preferred direction. In this particular design, the polarities are inverted relative to neuron membrane potentials, with inhibition represented by positive-going voltages and excitation by negative-going voltages. The input current was switched from cell to cell each 50ms, which would correspond to a 'speed' of 30 degrees per second if the 'cells' were associated with ommatidia with a separation angle of 1.5°. The time constant in the nonlinear filter circuit was set by hand so that signal decay is relatively slow compared to the 50ms transition time (whereas the onset is rapid enough to equilibrate in less than that time).

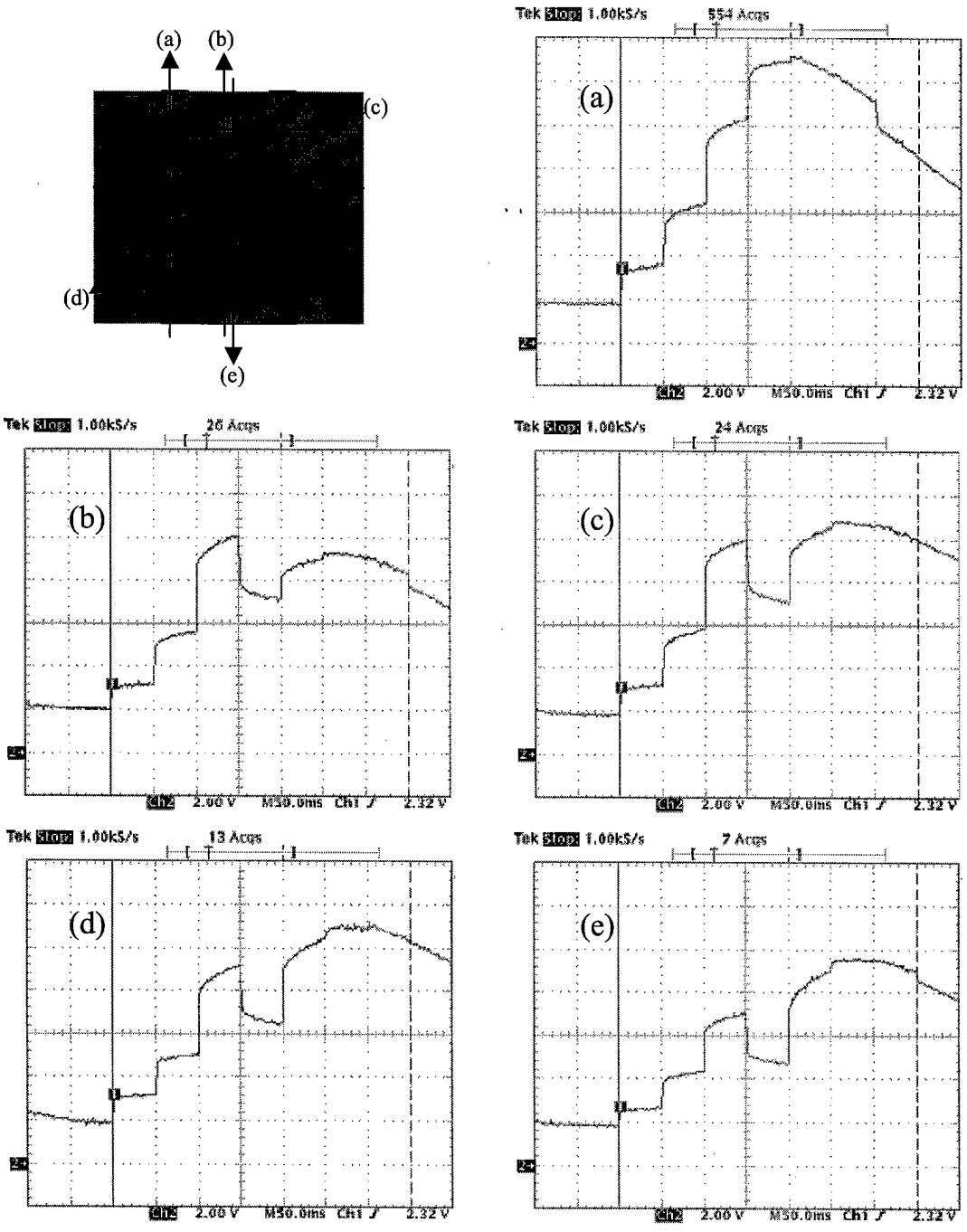

Figure 23: Results from the SOS ESTMD array. The icon at upper left shows the different paths across the ESTMD receptive field of the central cell, over which an input current pulse (a "moving target") was stepped. The excitatory center in this icon is depicted in red, with the preferred direction downward. Each trace shows the central ESTMD output for one of the input paths. Effective vertical scale is 1μA per division. Inhibition is represented by positive voltages and excitation by negative. 'Resting potential' is two divisions up from the bottom of each graph.

In the results in Figure 23, the excitation when the input crosses the receptive field center is not sufficient to overcome the effects of inhibition, even in the preferred direction. However, the results are qualitatively as desired, as the closest approach to net excitation does occur in the preferred-direction case (Figure 23e).

Interestingly, when new simulations of this circuit were run with abstract components replacing the active devices, the scaling mismatch observed between the excitatory and inhibitory currents was the *opposite* of what was seen experimentally: the simulated excitatory currents were too large relative to the inhibitory component, rather than the other way around. This is illustrated below in simulation results depicted in Figure 24. In these results, both preferred and antipreferred-direction stimuli resulted in net excitation (positive polarity in this case). Repeated examination and analyses of both the design and the simulated circuit failed to uncover any reason for this discrepancy: component scaling in both was found to be as assumed, and these two scalings matched. We concluded that there must be a systematic but non-design-related cause to the scaling problem. It might be due to systematic mismatch in transistor properties in the layout (caused, for example by transistor positions relative to other devices), or there might be another cause, such as a deviation from expected threshold that forces the excitatory transistors to operate in the triode mode and supply less than the expected amount of current. Either way, the discrepancy between simulated and actual behavior did not bode well for design efforts in SOS, and it became another significant factor in our ultimate decision to pursue subsequent designs in bulk silicon rather than SOS.

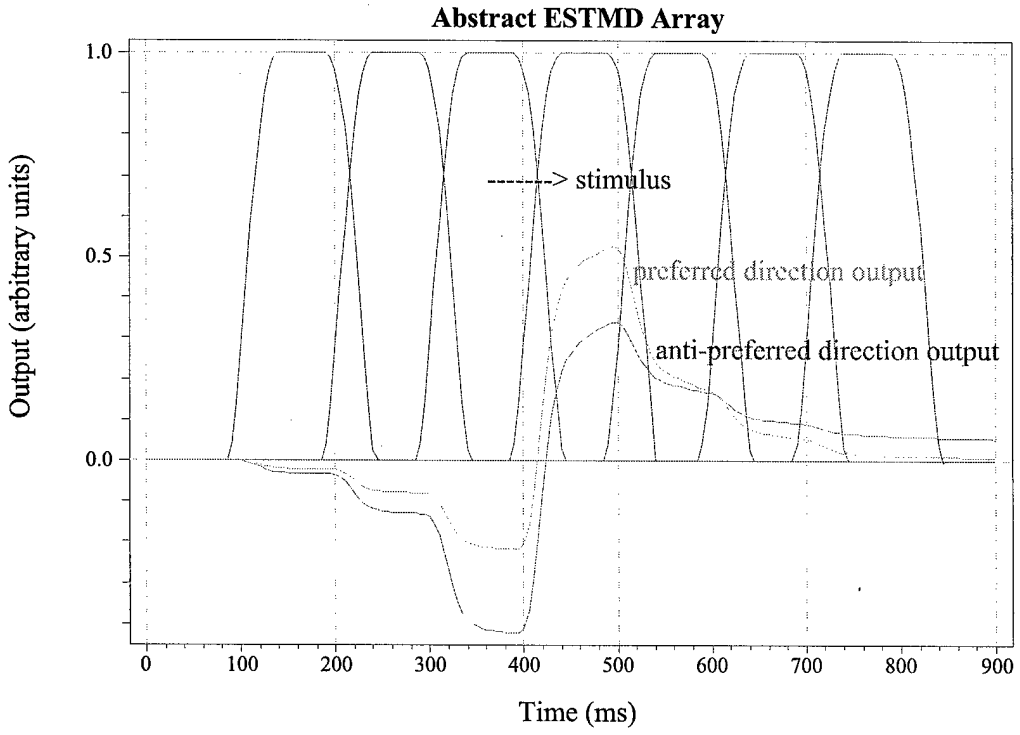

Figure 24: Simulated output of the SOS ESTMD array, with devices represented by abstract components. Output polarities are reversed with respect to the actual

circuit of Figure 23. The excitatory signal scaling is too large in this case for it to be overcome by inhibition when motion is in the antipreferred direction.

In the ESTMD array on ***chip_1_bulk***, the scaling issue received careful attention in design and simulation. Unfortunately, the version of the tonic filter included in the ESTMD cell on this chip had such long intrinsic time constants that it was not operable at practical frequencies on this chip, and testing of the ESTMD array on this chip proved to be infeasible.

The ESTMD cell used in the final test chip, ***ESTMD_chip***, included the redesigned version of the tonic filter depicted in Figure 21. This allows a 'tonic' response in the subthreshold regime, as well as controllability of the time constant. Nominal excitatory and inhibitory scaling values, as determined by simulation and analysis, were used in the primary test structure, under the assumption that the test results obtained from the SOS version of the circuit were anomalous. However, as a hedge, a second version of the ESTMD array was included in which the scaling of the excitatory signals was increased, so as to permit the circuit to function if in some way the required excitatory scaling was underestimated.

The ESTMD arrays on ***ESTMD_chip*** were be set up so that a cluster of seven adjacent ESTMD cells could be addressed at once, and supplied with seven independent inputs. This architecture allows the imposition of input sequences whose spatiotemporal signatures cover more than one pixel simultaneously. It was implemented to allow simulation of moving targets of sizes larger than a single pixel. In addition, some preprocessing schemes (such as the elementary motion detector) may result in signatures that are more than one pixel in spatial extent, even in response to single-pixel moving targets. This array will be implemented with a single preferred direction, as on the first pair of chips.

Preliminary results from the array with nominal current scaling were positive. In experiments using a single-pixel pulse stimulus moved across the array at a fixed speed (as in the prior chips), the 'tonic' filters could be tuned so that 'excitation' resulted when the stimulus moved in the preferred direction, but not when the stimulus moved in other directions. A set of example outputs is depicted below in Figure 25:

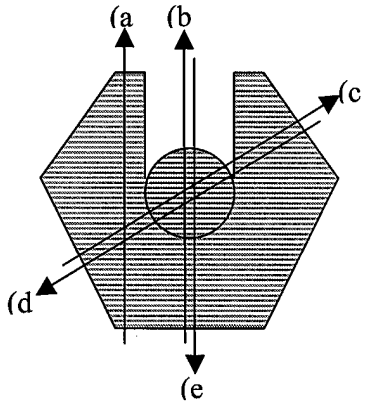
(a
(b
(c
(d
(e

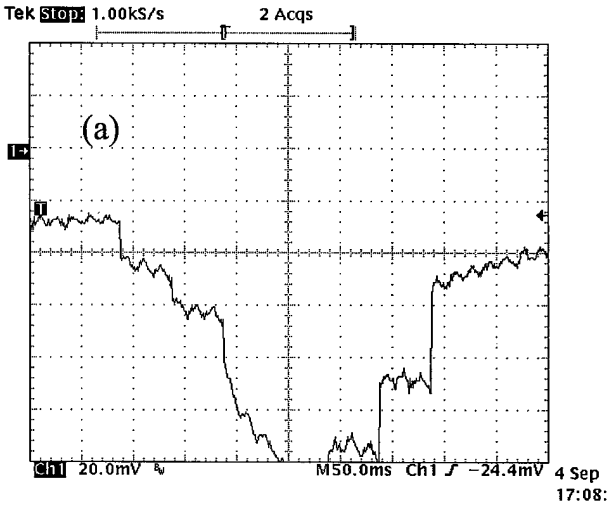
Tek Stop: 1.00kS/s 2 Acqs
(a)
Ch1 20.0mV M50.0ms Ch1 ƒ −24.4mV 4 Sep
17:08:

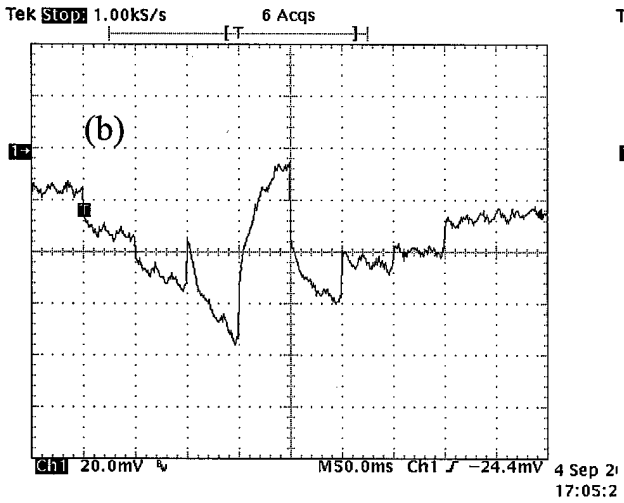
Tek Stop: 1.00kS/s 6 Acqs
(b)
Ch1 20.0mV M50.0ms Ch1 ƒ −24.4mV 4 Sep 2
17:05:2

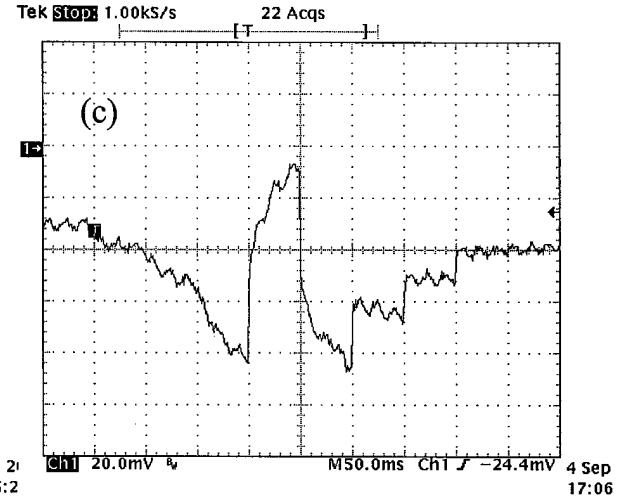
Tek Stop: 1.00kS/s 22 Acqs
(c)
Ch1 20.0mV M50.0ms Ch1 ƒ −24.4mV 4 Sep
17:06

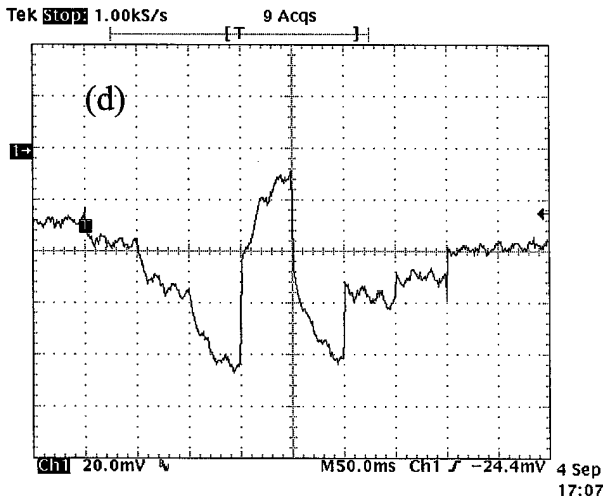
Tek Stop: 1.00kS/s 9 Acqs
(d)
Ch1 20.0mV M50.0ms Ch1 ƒ −24.4mV 4 Sep
17:07

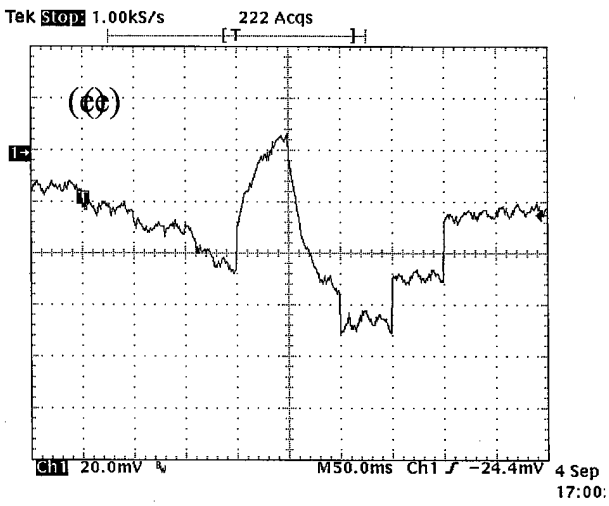
Tek Stop: 1.00kS/s 222 Acqs
(e)
Ch1 20.0mV M50.0ms Ch1 ƒ −24.4mV 4 Sep
17:00:

Figure 25: (Previous page) Results from the bulk silicon ESTMD array on *STMD_chip*. The icon at upper left shows the different paths across the ESTMD receptive field of the central cell, over which an input current pulse (a "moving target") was stepped. The excitatory center in this icon is depicted in red, with the preferred direction downward. Each trace shows the central ESTMD output for one of the input paths, as a function of time. Inhibition is represented by negative voltages and excitation by positive. 'Resting potential' is two divisions down from the top of each graph. The circuit was operated in weak inversion.

In the responses in Figure 7, only stimulus motion in the preferred direction yielded an excitatory (net positive) response when the stimulus crossed the center of the receptive field. Although this is as desired, the response is weak in magnitude and there is little margin between its peak and the peaks induced when the stimulus crosses the excitatory region in the non-preferred directions.

In an effort to improve the performance of the circuit, we also ran experiments in which it was operated in moderate inversion. Although this mode results in better noise margin, the difference between preferred- and non-preferred-direction responses remains modest relative to overall signal levels.

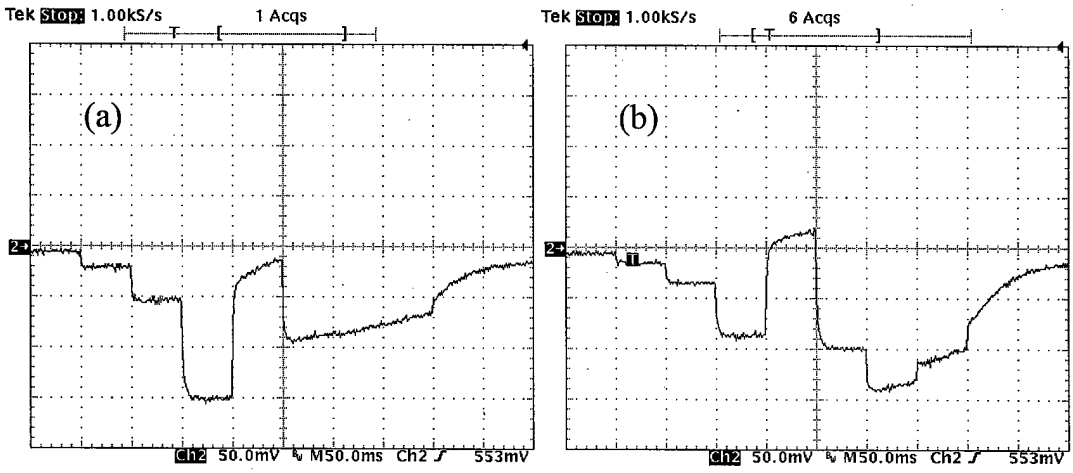

Figure 26: Response of bulk silicon ESTMD array on *STMD_chip* (version with nominal scaling of excitation and inhibition) as a function of time, to antipreferred (a) and preferred (b) direction 'small moving target' stimuli. The circuit is operated in moderate inversion.

When the second ESTMD array with increased scaling of excitatory current components was tuned so that preferred-direction stimuli resulted in net excitation, then stimuli crossing the excitatory center in any other direction also caused an excitatory response, demonstrating that the excitatory scaling is too large and confirming the suitability of scaling in the nominal array.

However, we investigated a mode of operation of the tonic filter that ultimately allowed the second array to function as desired. When the input of the filter is *overdriven*, that is, subject to voltages at which its current levels are saturated, then the

output enters a regime in which a nearly constant output persists after the end of the stimulus, until the gate voltage of the output device discharges below the saturation level. This is illustrated in Figure 27 below, in which the left panel demonstrates the step response of the filter in the normal 'tonic' mode, and the right panel, in the saturated mode:

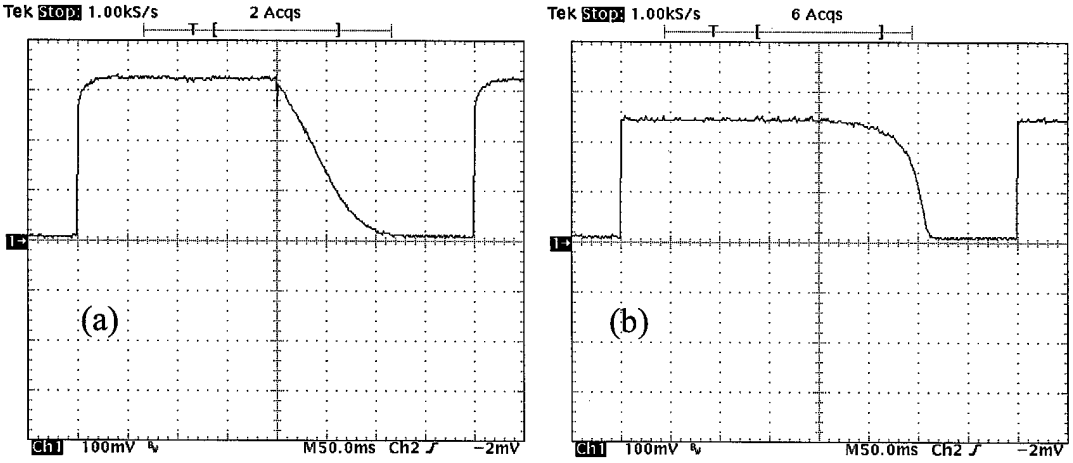

Figure 27: Step response of the cascaded subthreshold 'tonic' filter in the 'normal' tonic mode, (a), and in the saturated mode, (b).

When the filters in the second array are operated in the saturated mode and properly tuned, the persistence of inhibition at relatively high levels in the network allows supression of excitation by non-preferred-direction stimuli, while still permitting net excitation by preferred-direction stimuli. This is illustrated in Figure 28 below.

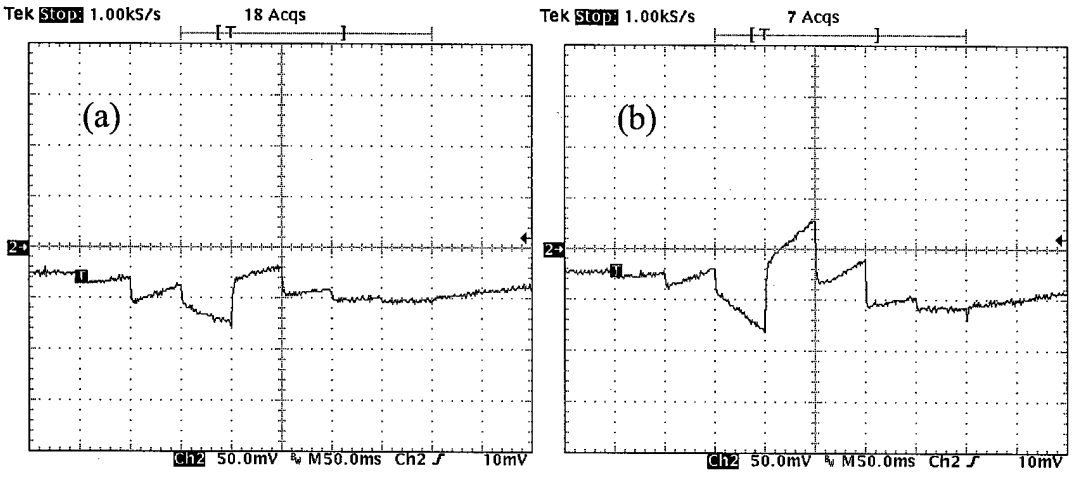

Figure 28: Response of bulk silicon ESTMD array on *STMD_chip* (version with increased excitatory scaling) as a function of time, to antipreferred (a) and preferred (b) direction 'small target' stimuli. The tonic filter is operated in saturated mode.

In the experiments on the ESTMD arrays, particularly when operated in subthreshold, we found these circuits to be subject to low-level, but long-lasting, residual 'inhibition,' which depresses the ESTMD output for relatively long periods after a stimulus event. On analysis, we attribute this to a design oversight: when the input to an ESTMD transitions from an addressed state to an unaddressed state, its input floats, and although the tonic filter discharges according to the desired time history at first, the discharge eventually slows due to the fact that the input transistor enters a high-impedance state and there is no low-impedance path for current leaving the integrating node of the filter. The filter continues to source small amounts of current onto the diffusive inhibitory network. This problem could be remedied by using a weakly-biased transistor to 'shut off' the ESTMD input device when there is no externally-applied input.

All of the results presented above were for single 'pixel' small targets moving at a particular speed (i.e., with a 50ms transition time per 'ommatidium'). When this speed was varied while retaining a fixed tuning of the STMD cells, we found that the desired response (net excitation in the preferred direction and that direction only) could be maintained for just a small range of speeds – varying by a factor of about two for the nominal array, and two to three for the second array when operated with tonic filters in 'saturated' mode. Because even in the 'normal' tonic mode, the filter decay (i.e., fall time) is on the order of ten times faster than the rise time, we would expect a broader range of speeds to be achievable. We believe that several factors negatively impact this speed tuning: the presence of persistent inhibition; non-optimality of the relative scaling of inhibition and excitation (the nominal array, while functional, should probably have somewhat greater excitation); and finally, the chosen architecture itself. While the use of only nearest-neighbor connections significantly simplifies the physical layout of the ESTMD circuits, permitting a broader range of interconnections would allow implementation of ESTMD models with better discrimination between preferred and

non-preferred direction stimuli, and broader velocity tuning as well. The simplest such elaboration may be to allow directed inhibition between both nearest and next-nearest neighbors.

Finally, the ESTMD arrays were tested using a moving stimulus consisting of three adjacent active 'pixels' rather than a single pixel stimulus. This stimulus was moved in the preferred direction, but it is broader than the effective 'notch' in the inhibitory receptive field. Accordingly, strong inhibition with no period of net excitation was observed during target transition, demonstrating the small-target selectivity of the model.

3.3.4 Collator Dendrite Model

In a second and larger set of arrays on ***ESTMD_chip***, we implemented ESTMD arrays with the single-pixel input architecture as on the initial chips, but with two preferred directions, corresponding to a set of ESTMDs aligned with two of the principal axes of the hexagonal array. In addition, we implemented analogs of dendritic processing that we assume may be present in collator cells corresponding to wide-field STMD neurons. This collation was not a simple summation. Rather, the (biologically plausible) approach we took consisted of circuits whose response is enhanced by the sequential excitement of ESTMDs along continuous tracks. Continuity of motion is an expected constraint for natural targets, and exploitation of this constraint could lead to higher-confidence detection of target motion.

The basic concept behind this approach is illustrated in the schematic diagram of Figure 29 below:

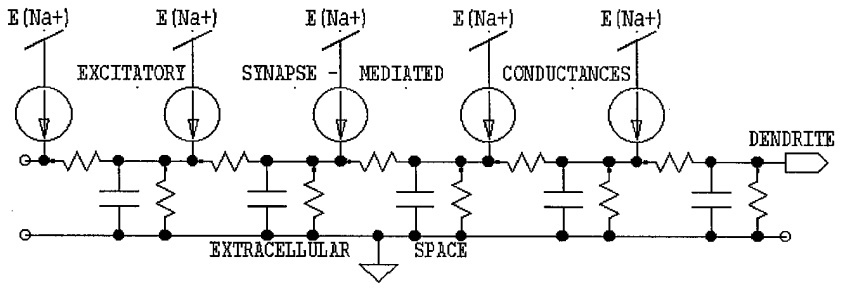

Figure 29: Dendrite analog. Membrane properties approximated by lumped parameters. Sequential activation of input synapses reinforces a diffusive wave of excitation in the dendrite.

The continuous membrane capacitance, resistance, and cytoplasmic resistances were modeled with lumped-parameter elements. Synaptic inputs were assumed to be from (retinotopically-organized) ESTMDs, and were modeled as excitatory and unipolar, i.e., they are active only when the corresponding ESTMD receives a spatiotemporal input that results in its excitation.

In the dendritic analogs of the STMD circuit, the first-order lowpass characteristic associated with each RC stage in Figure 29 was implemented with an active log-domain filter circuit, analogous to that in the ESTMDs. If the cascode transistors in this filter

circuit are turned full "on," and their input currents from the ESTMDs are at weak inversion levels, then they will act as linear filters, and signal propagation in the 'dendrite' will model a set of superposed diffusive responses. However, by adjusting the cascode bias, they may be operated in the same nonlinear 'tonic' mode as the circuits in the ESTMDs – fast excitation, slow decay of excitation – in order to mimic active membrane properties that might result in tonic behavior. This could be used to strengthen the reinforcement of a 'wave' of excitation. Naturally, we expedt the temporal tuning of the filters to be reflected in the velocity tuning of the 'dendrite,' and presumably it should be at least somewhat matched to the velocity tuning of the ESTMD cells at the front end.

In the STMD circuit appearing on the final test chip, individual 'dendritic' segments have retinotopic 'receptive fields' four stages long in the direction of motion sensitivity, and two ESTMDs wide. The wide-field STMD cells sum the outputs of 'dendrites' at several overlapping locations in the retinotopic array, and aligned with two principal directions of the hexagonal lattice, resulting in a somewhat broader direction selectivity (on the order of 60°) than the individual ESTMDs supplying its inputs.

Testing and diagnosis of the dendritic analog circuits was limited due to exhaustion of time and funds on the project. However, we present some representative results of the limited tests performed, below in Figure 30. In these experiments, the 'small target' stimulus was moved across the array in several directions, and the dendrite filter stages were biased the same as the ESTMD filters (i.e., in 'tonic' mode).

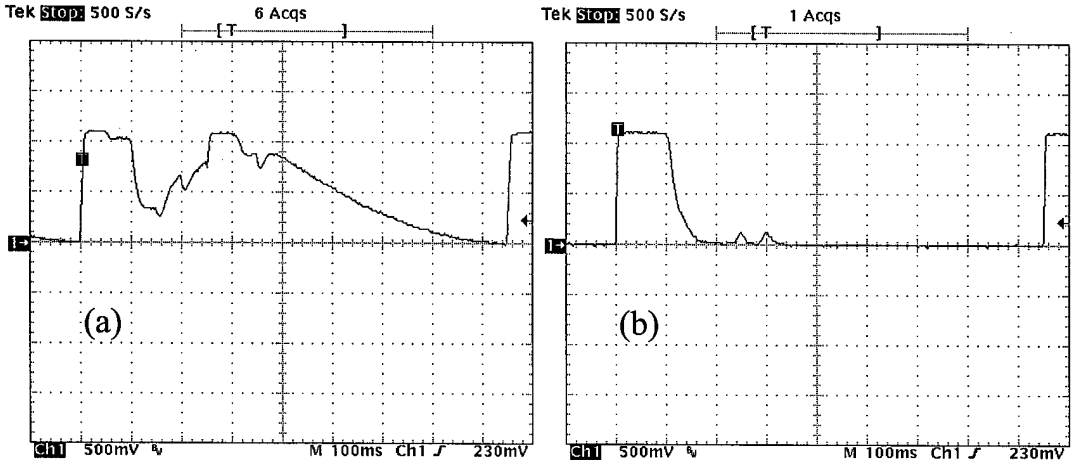

Figure 30: Response of an STMD 'dendrite' circuit to 'target' motion in its preferred (a) direction and a non-preferred (b) direction, as a function of time. In both cases, an artifactual initial excitation is present, followed by building excitation in the preferred direction, but only some small excitatory spikes in the non-preferred direction.

In these results, for as-yet undiagnosed reasons, there is a burst of excitation at the assertion of the first one or two addresses in the sequence used to steer the 'moving target' stimulus across the array (this artifact may be due to improper boundary conditions on the ESTMD cells in the array, leading to full excitation of the 'dendrite' containing these cells). Following this, excitation rebuilds in the case of the preferred

direction stimulus, dying away slowly after the end of the 'motion,' but in the non-preferred case, there are only a few 'breakthrough spikes' of excitation, presumably due to ESTMD outputs just momentarily reaching the threshold of excitation.

3.4 SUMMARY AND CONCLUSIONS

In the neurobiological portion of our work, we characterized the responses of a range of neurons that can be considered small target movement detectors; developed preliminary classifications for some of these cells, including a small-field STMD that we have labeled an 'elementary small target movement detector', or ESTMD, and which may be an early or intermediate stage in a hierarchy of STMD processing; discovered that at least some STMD neurons are capable of responding selectively to small moving targets against moving cluttered backgrounds; and obtained data from an STMD neuron that we believe will prove identifiable from individual to individual of a particular species (*E. tenax*).

In our modeling work, we developed conceptual and numerical models for the small-field STMD neurons that we have labeled ESTMDs; studied the responses of elementary motion detectors (the putative front-end for STMD neurons) to small target motion; developed a model for processing that could endow STMD neurons with selectivity for small target size in the direction of motion; examined possible mechanisms for collation of ESTMD outputs; and developed a revised hierarchy of STMD processing in view of the discovery of neurons capable of distinguishing moving targets against moving backgrounds.

In our effort to implement neuromorphic analog circuit models of STMDs, we evaluated primitive devices in two different CMOS processes (standard bulk silicon mixed-signal CMOS and silicon-on-sapphire); invented a novel log-domain filter circuit that can be operated in a nonlinear mode to mimic the 'tonic' property of ESTMD neurons; implemented, tested and demonstrated silicon models for the ESTMD; and implemented and performed pilot testing of a model for dendritic collation in a wide-field STMD analog.

4 PERSONNEL SUPPORTED

Patrick Shoemaker, Tanner Research, Inc., Co-Investigator
David O'Carroll, University of Adelaide, Co-Investigator
Roger DuBois, University of Adelaide, Post-Doctoral Fellow
Tamath Rainsford, University of Adelaide, Post-Doctoral Fellow (partial support)
Andrew Straw, University of Adelaide, Graduate Student (limited support)
Irene Moyer, University of Adelaide, Undergraduate vacation scholar
Thomas Bartolac, Tanner Research, Inc., Senior Scientist (limited support)

5 PUBLICATIONS

5.1 Publications Wholly or Partly Supported by this Contract

Shoemaker, P. A. (2003) A methodology for long time constant log-domain filters in CMOS. Submitted to *Analog Integrated Circuits and Signal Processing.*

DuBois, R.A., O'Carroll, D., and Shoemaker, P.A. (2003) Spatio-temporal tuning for small targets from a simulated array of elementary motion detectors, in N. Elsner & H. Zimmermann, Eds., *The Neurosciences – From Basic Research to Therapy: Proceedings of the 29th Göttingen Neurobiology Conference* (Germany), Georg Thieme Verlag, Stuttgart, pp. 547-548.

Shoemaker, P. A., O'Carroll, D. C., and Straw, A. D. (2001) Implementation of visual motion detection with contrast adaptation. *Proceedings of SPIE, Electronics and Structures for MEMS* (Adelaide, December 2001), Vol. 4591, pp. 316–327.

O'Carroll, D.C. (2001) Biomimetic visual detection based on insect neurobiology. *Proceedings of SPIE, Electronics and Structures for MEMS* (Adelaide, December 2001), Vol. 4591, pp. 1-10.

O'Carroll, D.C., and Henry, J. (2001) Visual detection of prey by dragonflies. Presented at the International Conference for Invertebrate Vision (Bäckaskog Castle, Sweden, August 7-12).

5.2 Publications in Related Fields by the Principals

O'Carroll, D.C., Straw, A.D., Shoemaker, P.A., and Rainsford, T. (2003) Adaptive gain control in insect motion detection, in N. Elsner & H. Zimmermann, Eds., *The Neurosciences – From Basic Research to Therapy: Proceedings of the 29th Göttingen Neurobiology Conference* (Germany), Georg Thieme Verlag, Stuttgart, pp. 546-547.

Straw, A.D. & O'Carroll, D.C. (2003) Ghosting and Aliasing Artifacts in Apparent Motion Displays Eliminated with Motion Blur, in N. Elsner & H. Zimmermann, Eds., *The Neurosciences – From Basic Research to Therapy: Proceedings of the 29th Göttingen Neurobiology Conference* (Germany), Georg Thieme Verlag, Stuttgart, pp. 601-602.

DuBois, R.A., Engel N. and Stuart G. (2003) Design and construction of a dynamic clamp device for biological neurons, in N. Elsner & H. Zimmermann, Eds., *The Neurosciences – From Basic Research to Therapy: Proceedings of the 29th Göttingen Neurobiology Conference* (Germany), Georg Thieme Verlag, Stuttgart, p. 1059.

DuBois, R.A., Engel N. and Stuart G. (2003) Transient synchronization of cortical neurons using synthetic conductance, in N. Elsner & H. Zimmermann, Eds., *The Neurosciences – From Basic Research to Therapy: Proceedings of the 29th Göttingen Neurobiology Conference* (Germany), Georg Thieme Verlag, Stuttgart, p. 583.

DuBois, R.A. (2003) Bifurcation between quasi-stationary cortical activity states alters the spatial and temporal distribution of response patterns, in N. Elsner & H. Zimmermann, Eds., *The Neurosciences – From Basic Research to Therapy: Proceedings of the 29th Göttingen Neurobiology Conference* (Germany), Georg Thieme Verlag, Stuttgart, p. 582.

Harris, R.A., and O'Carroll, D.C. (2002) Afterimages in fly motion vision. *Vision Research* Vol. 42, pp. 1701-1714.

Straw, A.D., O'Carroll, D.C., & Shoemaker, P.A. (2002) Adaptive Motion Detectors Inspired by Insect Vision. *Proceedings of the First World Congress on Biomimetics and Artificial Muscles* (Albuquerque, NM, December 9-11).

DuBois, R.A. (2001) Optomotor reafference to the medulla and object tracking. Presented at the International Conference for Invertebrate Vision (Bäckaskog Castle, Sweden, August 7-12).

6 INTERACTIONS / TRANSITIONS

6.1 Participation / presentation at meetings, conferences, and seminars

David O'Carroll and Patrick Shoemaker held a collaborator's meeting, including O'Carroll lab members R. DuBois, T. Rainsford, and A. Straw, at the University of Adelaide, 21-31 October 2003. During this period, O'Carroll and Shoemaker met with COL Don Erbschloe, commanding officer, AFOSR, and MAJ Tony Mitchell, Technical director at AOARD, on a site visit to Adelaide.

Patrick Shoemaker attended the attended the AFOSR Dynamics and Control contractors/grantees meeting held 9-11 September 2003 in Destin, FL.

David O'Carroll made a two-week visit in May-June 2003 to his former laboratory in England at the University of Cambridge (host Prof. Simon Laughlin), and presented a research seminar.

David O'Carroll visited the University of Bonn, Germany, in June 2003 (host Prof. Gerhard von der Emde) and presented a research seminar.

David O'Carroll, Roger DuBois, and Andrew Straw attended the 29th Göttingen Neurobiology Conference in June 2003, and presented a number of posters.

Roger DuBois attended the 5th meeting of the German Neuroscience Society in June 2003.

Roger DuBois met with European neuroscience and biomimetics researchers, including: Tobi Delbrück and Shih-Chii Liu at the Institut für Neuroinformatik, University of Zürich / ETH Zürich; Prof. Henry Markram at the Brain Mind Institute at the Ecole Polytechnique Fédéral de Lausanne; Prof. Egbert Welker at the Institut de Biologie Cellulaire et de Morphologie, Lausanne; and Prof. Greg Stuart, University of Freiburg, Physiology I, Freiburg, Germany, in June 2003.

David O'Carroll and Patrick Shoemaker held a collaborator's meeting at the University of Adelaide, 4-13 September 2002.

Patrick Shoemaker attended the AFOSR Dynamics and Control contractors/grantees meeting held 12-14 August 2002 in Pasadena, CA, and presented a poster describing work on this project.

Jordanna Henry (graduate student in the former O'Carroll lab at University of Washington) visited the O'Carroll lab in April-May 2002 to analyze accumulated data for STMD responses.

Patrick Shoemaker attended AFOSR Workshop on Future Direction in Control, held 26-27 April 2002 in Arlington.

Patrick Shoemaker presented a seminar entitled "Modeling adaptation in insect visual motion processing" at the University of Maryland on 25 April 2002 (hosted by fellow AFOSR grantee P.S. Krishnaprasad).

David O'Carroll and Patrick Shoemaker attended the Symposium on Microelectronic and Micro-Electro-Mechanical Systems, held 17-19 December 2001 in Adelaide. O'Carroll presented a plenary lecture entitled "Biomimetic visual detection based on insect neurobiology," and Shoemaker presented a poster entitled "Implementation of visual motion detection with contrast adaptation."

Patrick Shoemaker attended the Conference on Cooperative Control and Optimization and AFOSR Cooperative Control Theme kickoff meeting held 12 - 14 November 2001 at the University of Florida in Gainesville, FL.

David O'Carroll and Jordanna Henry attended the International Conference on Invertebrate Vision, held at Bäckaskog Castle, Sweden, 7 – 12 August 2001. Henry presented a poster entitled "Visual detection of prey by dragonflies."

Roger DuBois attended the International Conference on Invertebrate Vision, held at Bäckaskog Castle, Sweden, 7 – 12 August 2001, and presented a poster entitled "Optomotor reafference to the medulla and object tracking."

Patrick Shoemaker attended the AFOSR 2001 Grantees/Contractors Meeting for Dynamics and Control, held 30 July - 2 August 2001 at Wright-Patterson AFB, Dayton, OH.

6.2 Consultative and advisory functions

From late 2002 until the present, David O'Carroll has acted as a liason with officials at the Weapons Systems Division (WSD) of Australia's Defence Science and Technology Organisation (DSTO) to investigate mutual interests in guidance and control. WSD supports biomimetic work at Australian National University (Srinivasan & colleagues) where they presently fund a UAV project. As a result of these efforts, (and relying on materials provided with the support of this AFOSR Themes contract), Dr. Farhan Faruqi at DSTO has indicated the intention of funding a key initiative in Biomimetics. DSTO intends to support a full salary for a Scientist at Adelaide University, as well as a similar funding level for ANU. This will be an initial 3 year seed project, but with a view to establishing permanent funding for a centre of excellence (COE) in Biomimetics to be based in Adelaide. Funding is currently on hold; however, this initiative will eventually represent a substantial opportunity to leverage funds supplied by the US Air Force.

6.3 Transitions

Tanner Research (Shoemaker) in partnership with the University of Adelaide (O'Carroll) in March 2003 were awarded a Navy Phase I SBIR project, entitled "Insect Small Target Motion Detection for Seeker Applications." The contract number is N00014-03-M-0171, and the COTR, Dr. Ron Scott, Code 472100D, NAWCWD, China

Lake, CA 93555, phone (760) 939-4002. The proposed work relied heavily on accomplishments under this AFOSR Themes contract, and the two efforts have been closely complementary. During this project, we examined in greater detail the responses of STMD cells to small moving targets against stereotypic moving clutter, in the context of a realistic DoD application (an air-to-ground platform). However, the work did not transition to a Phase II project.

In early 2003, David O'Carroll was successful in application for a full faculty position at the University of Adelaide. The funds that had previously provided salary support (under an Air Force contract international research initiative (IRI) contract) were freed up and enabled the appointment of a new Post-Doctoral Fellow, Dr. Tamath Rainsford, with a background in Physics and Neurobiology. Dr. Rainsford has contributed substantially to experimental work performed under this contract during 2003.

7 Inventions and Patent Disclosures

A novel concept for a log-domain lowpass filter circuit was conceived and reduced to practice under support of this project. This circuit is capable of implementing very long (biological) time constants, and in addition may be operated in a nonlinear mode in which it is useful for the simulation of dynamic processes with fast onset and slow decay (an important component of small target-detecting models). A paper describing the invention has been written and is under final review at the journal Analog Integrated Circuits and Signal Processing. With the statutory bar imposed by this publication, Tanner Research Inc. expects to initiate the filing of a patent on the invention in the near future. A DD Form 882 is included herewith.

During development of the stimulus system supported in part by this project, Andrew Straw and David O'Carroll developed a novel motion animation technique that reduces image ghosting (a form of temporal aliasing) in apparent motion presentations. The method was optimized through a model for the physiological mechanisms of temporal blur introduced by biological photoreceptors. Although originally developed to remove ghosting artifacts from stimulus sequences presented to insects during experimentation, the method has widespread potential applications in real-time computer animations for human observers (including video games). A provisional patent was filed with the Australian Patent Office (provisional no 2002952815), and has subsequently lapsed. We are presently finalizing a manuscript detailing the theory underlying the method and are considering seeking US patent protection.

8 Honors / Awards

The poster presented by Henry mentioned in Sections 5.1 and 6.1 above was runner-up prize-winner for the best student presentation at the 2001 International Conference on Invertebrate Vision.

Bibliography

[1] Harris, R.A., O'Carroll, D.C. & Laughlin, S.B. (2000) Contrast Gain Reduction in Fly Motion Adaptation. Neuron vol. 28, pp. 595-606.

[2] Hassenstein, B., and Reichardt, W. (1956) Systemtheoretische analyse der Zeit-, Reihenfolgen-, und Vorseichenauswertung bei der Berwegungsperzeption des Rüsselkäfers Chlorophanus, Z. Naturforch. Vol. 11b, pp. 513-524.

[3] James, A.C. (1990) White noise studies in the fly lamina, PhD thesis, Australian National University, July 1990.

[4] Lipetz, L. E. (1971). The relation of physiological and psychological aspects of sensory intensity. In W. R. Lowenstein (Ed.),Handbook of sensory physiology (Vol. 1, pp. 191–225). New York: Springer-Verlag.

[5] Mead, C. *Analog VLSI and Neural Systems*, Addison-Wesley, Reading, MA, 1989.

[6] Naka, K. I., & Rushton, W. A. H. (1966). S-potentials from luminosity units in the retina of fish (cyprinidae). Journal of Physiology, London, 185, 587–599.

[7] O'Carroll, D.C. (2001) Motion adaptation and evidence for parallel processing in the lobula plate of the bee-fly Bombylius major. In Zanker, J.M., Zeil, J., (Eds.) Motion Vision, Computational, Neural, and Ecological Constraints. Springer Verlag, Berlin, Heidelberg & New York, pp. 381-394.